Microbial Cell Factories

RESEARCH

Open Access

Green synthesis of silver nanoparticles (AgNPs) from *G. stearothermophilus* GF16: stable and versatile nanomaterials with antioxidant, antimicrobial, and catalytic properties

Alessia Di Fraia[1], Giovanni Dal Poggetto[2], Michela Salamone[1], Federica Carraturo[1], Patrizia Contursi[1], Marco Guida[1], Danila Limauro[1], Viviana Scognamiglio[3], Manuela Rossi[4] and Gabriella Fiorentino[1*]

Abstract

Background Silver nanoparticles (AgNPs) have attracted considerable interest for their distinctive physicochemical properties and wide-ranging applications in nanomedicine, environmental catalysis, and antimicrobial applications. However, sustainable and robust biosynthesis methods remain a challenge.

Results In this study, we report the biosynthesis of thermostable AgNPs using the secretome of *Geobacillus stearothermophilus* GF16, a thermophilic and metal-resistant bacterium isolated from the hydrothermal volcanic area of Pisciarelli, Italy. The synthesis was performed without specialized growth media, relying solely on the cell-free bacterial supernatant, and was systematically optimized by varying precursor concentration, temperature, pH, and reaction time. The nanoparticles were characterized by UV-Vis spectroscopy, dynamic light scattering, Fourier-transform infrared spectroscopy, scanning (SEM) and transmission (TEM) electron microscopy. Morphological analysis showed predominantly subspherical nanoparticles with average diameters of 17 ± 5 nm (SEM) and 16 ± 5–7 nm (TEM), depending on precursor concentration. Thermogravimetric analysis demonstrated excellent thermal stability with retention of structural integrity up to 120 °C, an exceptional feature among biogenic AgNPs. The obtained AgNPs exhibited remarkable radical scavenging activity, reaching up to 79% in DPPH and 75% in ABTS assays at 100 µg/mL, highlighting a level of antioxidant performance rarely observed in AgNPs of bacterial origin. In addition to their redox properties, the nanoparticles demonstrated efficient catalytic activity as evidenced by the complete degradation of Congo Red in 20 min and 4-nitrophenol in 35 min. Time-kill assays and minimum inhibitory concentration (MIC) also showed a broad-spectrum antimicrobial potential with complete inhibition of *Staphylococcus aureus*, *Pseudomonas aeruginosa*, and *Salmonella Typhimurium* at 100 µg/mL. Interestingly, MIC values were significantly lower than those reported for comparable AgNPs. Notably, the nanoparticles also displayed hemocompatibility, validated by hemolysis

*Correspondence:
Gabriella Fiorentino
fiogabri@unina.it

Full list of author information is available at the end of the article

assays performed on both healthy and β-thalassemic erythrocytes, with hemolysis rates consistently below the 2% safety threshold.

Conclusions Overall, this study presents the first comprehensive characterization of AgNPs biosynthesized by a thermophilic bacterium, highlighting their multifunctional potential. The use of a thermophilic bacterium as a robust and flexible microbial nanofactory offers a novel eco-friendly and scalable strategy for AgNP production. The resulting nanoparticles exhibit unique thermal stability, broad-spectrum bioactivity, and clinically relevant hemocompatibility, underscoring their promising applicability in nanomedicine, green catalysis, and environmental remediation.

Keywords Silver nanoparticles, Extremophiles, Nanofactory, Antimicrobial activity, Catalytic efficiency, Biocompatibility

Graphical Abstract

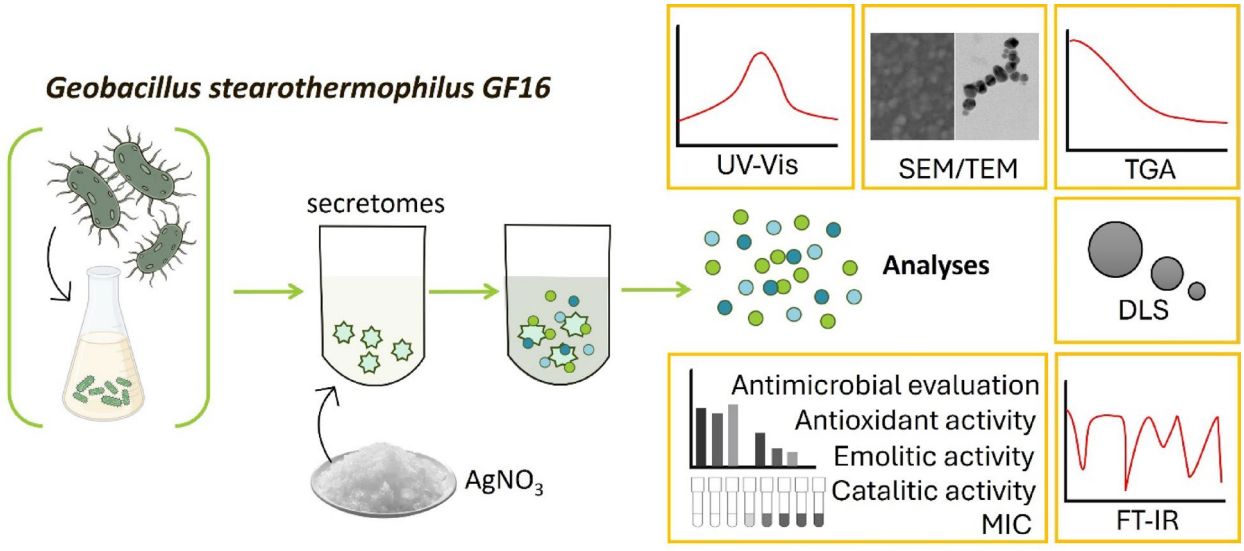

Background

Nanotechnology, which enables the manipulation of matter at the atomic and molecular scale, is emerging as an increasingly promising alternative to traditional technologies [1]. However, conventional nanomaterial synthesis methods, based on chemical and physical processes, have significant sustainability limitations, requiring high energy consumption and generating toxic byproducts [2].

In this context, biosynthesis of nanomaterials through living organisms is gaining recognition as a green alternative, utilizing plant extracts, bacteria, fungi, and algae to produce nanoparticles under milder conditions and without harmful reagents. This approach not only minimizes environmental impact but also enhances biocompatibility and stability, expanding applications in biomedical, environmental, and industrial fields. Moreover, biosynthesis contributes to reducing hazardous chemicals, aligning with the United Nations Sustainable Development Goals (SDGs), particularly in health (SDG 3.9), water quality (SDG 6.3), and ecological waste management (SDG 12.4) [3, 4].

Due to their extremely small size, ranging between 1 and 100 nm, nanoparticles exhibit a high surface-to-volume ratio, which enhances their chemical, physical, and biological reactivity compared to macroscopic materials [5, 6]. These unique properties make nanoparticles suitable for numerous applications, including medicine, electronics, and environmental sustainability [7–9].

Among the various types of nanoparticles, metal nanoparticles (such as gold, platinum, and silver) have demonstrated their ability to interact with biological systems and catalyze chemical reactions [10–13]. For example, a recent study by Kajani et al. [14] highlighted that gold nanoparticles exhibited strong anticancer activity against breast, ovarian, and cervical cancer cells, with low toxicity to healthy cells, making them promising therapeutic agents for targeted cancer treatments. Another recent study by Dang et al. [15] demonstrated the potential of AuNPs as colorimetric probes for detecting Fe^{3+} ions, marking an important step towards developing innovative sensors capable of rapidly and accurately detecting toxic contaminants in water. A recent study demonstrated that AgNPs conjugated with herbicides like imazapic and imazapyr, can function as innovative nanopesticides; these systems enable the controlled

release of active ingredients, making them more effective and environmentally friendly compared to conventional pesticides [16]. In a study conducted by Jeyaraj et al. [17], it was observed that platinum nanoparticles (PtNPs) have significant potential as therapeutic and diagnostic agents in the biomedical field. PtNPs have shown effectiveness as nanocarriers and nanosensors for diagnosis, in addition to displaying synergistic effects when used in combination with anticancer drugs at low concentrations. Compared to other types of nanoparticles, such as ceramic, carbon-based, or polymeric nanoparticles, metal nanoparticles offer significant advantages in terms of electrical conductivity, making them also particularly suitable for electronic applications and the production of conductive materials [18, 19].

Their use has also been reported in the development of advanced sensors, imaging techniques, and medical therapies, owing to their plasmonic properties and their ability to be easily functionalized with various chemical groups. This functionalization enhances their therapeutic targeting capacity and biocompatibility [20, 21].

Among metal nanoparticles, AgNPs have proven to be highly versatile, finding applications in a wide range of fields, including antimicrobial coatings for medical devices, water purification technologies [22], and the production of biosensors for electronics and bioimaging [23]. Recent studies, such as the one conducted by Jangid et al. [24], have demonstrated that AgNPs synthesized via biological methods can enhance antimicrobial efficacy in wound treatment, while Biswas et al. explored their use in chemical catalysis for environmental purification [25].

Nanoparticle synthesis can primarily be achieved through two approaches: the "Top-Down" method, which involves breaking down larger materials into nanoscale sizes, and the "Bottom-Up" method, which utilizes the aggregation of elemental units such as atoms or molecules. The latter is often preferred due to the greater control it offers over particle morphology and can be performed through chemical and biological techniques [26]. However, while chemical techniques may require the use of toxic reagents, biological techniques represent a more sustainable alternative, as synthesis occurs using living organisms like bacteria, algae, fungi, and plant extracts [5, 27, 28]. For instance, in a study conducted by Hossain et al., biogenic AgNPs were successfully synthesized using *Phyllanthus emblica* pulp extract, which conferred excellent antibacterial activity against both pathogenic and non-pathogenic strains. The biogenic AgNPs demonstrated hemocompatibility and biocompatibility, with no significant toxic effects on the liver and kidneys, highlighting their great potential as safe and versatile antimicrobial agents for the treatment of bacterial infections [29–31].

While plants and fungi have long been studied for their ability to synthesize AgNPs, the potential of bacteria in this context has gained significant attention in more recent years. Their ease of cultivation, rapid growth, and dual role as reducing and stabilizing agents make them highly suitable for efficient and scalable nanoparticle synthesis [33–35]. Moreover, bacterial biosynthesis often results in AgNPs with superior physicochemical properties compared to those obtained through conventional chemical methods. These nanoparticles typically exhibit more uniform and controlled size, greater colloidal stability due to natural biomolecular capping, and enhanced surface reactivity. AgNPs synthesized from extracellular bacterial secretomes are frequently coated with proteins, peptides, and other organic compounds that prevent aggregation and enhance biological and catalytic performance. These natural surface decorations also help mitigate the cytotoxicity of silver ions, promoting safer interactions with biological systems. In contrast, chemically synthesized AgNPs tend to be less stable and often lack biofunctional properties [32].

Even more recently, extremophilic bacteria have attracted attention as promising platforms for nanoparticle biosynthesis, owing to their unique metabolic pathways and ability to thrive in harsh environments, allowing the synthesis of nanoparticles across a wide range of parameters that are often inaccessible with traditional techniques and potentially offering advantages such as improved nanoparticle stability and functionality [33]. Microorganisms inhabiting habitats characterized by high metal concentrations have developed specific survival strategies, including enhanced metal tolerance and efficient detoxification systems such as the enzymatic or redox-mediated reduction of metal ions into less toxic, stable nanoparticles [34, 35].

Among extremophiles, the synthesis of silver nanoparticles (AgNPs) by *Geobacillus spp* has already been reported in the literature [36]. However, to the best of our knowledge, optimal production conditions have not yet been defined, nor has a comprehensive investigation of the biological properties of the resulting nanoparticles been conducted.

The aim of this study was to optimize the extracellular synthesis of AgNPs and to perform an in depth characterization of their physicochemical features, stability, and functional properties, using *Geobacillus stearothermophilus* GF16; it is a thermophilic and metal-resistant strain isolated by our group from the hydrothermal volcanic area of Pisciarelli (Naples, Italy), an extreme environment characterized by high temperatures and elevated concentrations of toxic metals such as cadmium and arsenic [37]. Its ecological origin and physiological features suggest an intrinsic capacity of metal biotransformation, which, combined with its fully sequenced genome, makes

it an excellent candidate for further molecular and functional studies [38]. Furthermore, despite prior investigations on other *Geobacillus* strains, *G. stearothermophilus* GF16 remains largely unexplored for nanoparticle production [36].

By establishing a tunable, efficient and scalable biosynthesis protocol, this study contributes to the development of robust and environmentally sustainable microbial cell factories to produce multifunctional nanomaterials.

Methods

Source of microorganism

In this study, the thermophilic bacterium *G. stearothermophilus* GF16, was used to synthesize AgNPs. The microorganism was initially isolated from the hydrothermal volcanic area of Pisciarelli, near Naples, Italy, identified and phenotypically characterized [37] and its genome was later sequenced and annotated (NCBI Accession: NZ_RCTI01000001) [38].

Growth and secretome production

A cryopreserved stock of *G. stearothermophilus* GF16 was thawed from storage at -80 °C and streaked onto Lysogeny Broth (LB) agar plates. The LB agar was made by using 10 g/L tryptone, 10 g/L sodium chloride, 5 g/L yeast extract, and 15 g/L agar. Plates were incubated at 60 °C for 16 h. A single colony was then picked up and transferred into liquid LB medium, incubated at 60 °C and shaken at 180 rpm for an additional 16 h. An aliquot of this culture was used to inoculate the main culture, adjusted to an initial optical density (A_{600}) of 0.1. The main culture was shaken at 180 rpm and 60 °C in an orbital shaker (New Brunswick™ Innova® 42 Series). After 24 h of incubation, cells were harvested by centrifugation at 2,500 g for 10 min. The supernatant was further centrifuged at 37,500 g for 40 min at 4 °C using a Beckman centrifuge with a JA25-50 rotor (Beckman Coulter, Avanti™ JA25-50) to remove any remaining cell debris, thus obtaining the cell-free secretome.

AgNP production, isolation, and purification

For the synthesis of AgNPs, aliquots of 7 mL of the collected secretome were transferred into tubes and treated with $AgNO_3$ (Sigma Aldrich) at concentrations of 0.25 mM, 0.5 mM, 1 mM and 2.0 mM. A cell-free secretome without $AgNO_3$ was used as a control, and a solution of $AgNO_3$ alone was used as an additional control. To determine the optimal synthesis conditions to obtain high yield and controlled nanoparticle size, key parameters were systematically evaluated in a stepwise approach. The evaluated parameters were the following: temperature (25, 37, 60, 70, and 80 °C), pH (5.0, 8.0, 12.0) and reaction time (24 and 48 h).

After synthesis, the secretomes were centrifuged at 37,500 g for 35 min, and the pellets were washed twice with deionized water, followed by centrifugation at 2.500 g for 15 min to eliminate unreacted silver ions. The AgNP pellet was then resuspended in 1 mL of distilled water and stored at 4 °C. Subsequently, before further analyses, the suspensions were lyophilized using a freeze-dryer (Heto PowerDry PL6000 Thermo Scientific) and subjected to ultrasonic treatment for 30 min (Digital ultrasonic DU 32- ARGOLAB).

From this point onward, the purified AgNPs obtained by incubating the secretomes at 60 °C and pH 8 for 24 h with 0.5 mM $AgNO_3$ are referred to as AgNP0.5, while those obtained under the same conditions using 2 mM $AgNO_3$ are referred to as AgNP2.0.

UV-Vis spectroscopy

The synthesis of AgNPs was monitored using UV-Vis spectroscopy. Absorption spectra of cell-free secretomes treated with $AgNO_3$ at all the tested conditions described above were recorded over a wavelength range of 200–800 nm using a UV-Vis spectrophotometer (Agilent Varian Cary 50) with 0.5 ml quartz cuvettes (Hellma Analytics, 10 mm path length). Spectra of cell-free secretome without $AgNO_3$ and a solution of $AgNO_3$ alone were used as controls.

Dynamic light scattering (DLS) and zeta potential measurements

The hydrodynamic diameter of the produced nanoparticles, the polydispersivity index ($Đ$) and zeta potential (ζ) were measured by DLS technique using a Zetasizer Nano ZS instrument (Malvern Instruments Ltd). All the samples were prepared in an identical manner. AgNPs were resuspended in distilled water ($\simeq$1 mg/ml) and placed in 1 ml cuvette. Each analysis was performed in duplicate and an average of three measurements is reported along with the standard deviation (SD).

For measuring the zeta potential of the produced nanoparticles, the latter were resuspended with distilled water in 1 ml final volume ($\simeq$1 mg/ml). The samples were filled in the capillary cells (DTS1070) and placed in the instrument sample holder. Each analysis was performed in duplicate and an average of three measurements is reported along with SD.

Fourier transform infrared spectroscopy (FTIR)

FTIR analysis was performed using a Perkin-Elmer Model GX spectrometer, with a resolution of 2 cm^{-1} and 60 scans across a frequency range of 400 to 4000 cm^{-1}. Prior to the analysis, KBr disks were prepared by mixing 3.00 mg of AgNP0.5 and AgNP2.0, with 197.00 mg of KBr. FTIR spectra were recorded and analyzed with

Origin software (v.2022b, Origin Lab Corporation, Northampton, MA, USA).

Thermogravimetric analysis (TGA)

To assess nanoparticle stability, TGA was performed using a Perkin-Elmer Pyris Diamond TGA/DTA analyzer (Milan, Italy) equipped with a gas control station. Prior to analysis, each sample was dried overnight under reduced pressure with desiccant salts to eliminate residual moisture. The dried samples (≃ 3–4 mg) were then placed in open ceramic crucibles and subjected to an isothermal treatment. The temperature gradually increased from 25 to 120 °C at a rate of 10 °C/min under a nitrogen flow of 30 mL/min. Once at 120 °C, the temperature was maintained for 30 min to simulate autoclave sterilization conditions. All measurements were performed in duplicate to ensure reproducibility.

TEM and SEM analysis of AgNPs

The size and morphology of AgNP0.5 and AgNP2.0 were examined by scanning electron microscopy (FeSEM) and TEM.

An Electron Microscope Field emission Zeiss Merlin VP Compact with camera Gemini equipped with a charge compensation system and with Oxford Instruments Microanalysis EDS (Energy Dispersive X-ray Spectroscopy) X- max 50, was used for morphological analyses of the samples. Data imaging processing was performed using the dedicated software SmartSem. The samples were metalized with gold and palladium using a sputter coater. A TEM using an EI TECNAI G^2 microscope operating at 200 kV (Fei Company, Drive, Hillsboro, CA, USA). For TEM imaging, 3 µL of dispersed AgNPs aqueous solution were dropped on a carbon-coated copper grid and air-dryed before imaging. The size of the nanoparticles was measured using NIS-Elements D 3.1 software (Nikon Instruments Inc., Tokyo, Japan). For the statistical analyses related to sample sizes, 100 nanoparticles were measured for either AgNP0.5 and AgNP2.0 and for each technique (FeSEM and TEM).

Antioxidant activity

The antioxidant activity of AgNP0.5, AgNP2.0 and the secretome was assessed using two well-established antioxidant assays: DPPH and ABTS, described in previous studies [17, 39, 40]. Lyophilized AgNPs at concentrations of 25, 50, 75, and 100 µg/mL, were subjected to ultrasonic treatment for 30 min and tested in the antioxidant assays. The scavenging activity (%) was calculated for all the samples using the following formula:

$$\text{Scavenging activity } (\%) \left[\frac{A_{control} - A_{sample}}{A_{control}}\right] \times 100 \quad (1)$$

DPPH assay

The DPPH assay evaluates the ability of samples to neutralize the DPPH radical (2,2-diphenyl-1-picrylhydrazyl), which changes color from purple to yellow upon reduction. This assay was performed following the method by Chu and Chen [41]. 25 µL of AgNPs or secretome solution and 225 µL of DPPH solution (200 µM) prepared in methanol were added in a 96-well microtiter plate; the plates were incubated in the dark at room temperature for 30 min before measuring absorbance at 517 nm in a multiplate reader (BioTek Synergy HTX Multimode Reader). Methanol served as the blank, while DPPH solution without AgNPs or secretome, was used as the control. The scavenging capacity was calculated using the formula (1). Trolox was used as a standard at concentrations ranging from 5 to 100 µM.

ABTS assay

The ABTS radical scavenging activity was also evaluated following the method described by Xiao et al. [42], with slight modifications. In water, ABTS absorbs light at 734 nm, but absorbance decreases in the presence of antioxidants, as the ABTS radical cation is terminated. 200 µL of $ABTS^+$ solution and 10 µL of each sample were mixed in a 96-well microtiter plate and incubated in the dark for 7 min at room temperature, before measuring the absorbance at 734 nm wavelength (BioTek Synergy HTX Multimode Reader). Trolox was used as a standard reference at concentrations ranging from 0.2 to 0.8 µg/mL, while distilled water served as the blank control. The samples were appropriately diluted to ensure that the absorbance values fell within the specified range.

Hemolytic activity of AgNPs

The hemolytic activity of AgNPs was evaluated using human erythrocytes and monitoring hemoglobin release during the incubation under simulated physiological conditions [43, 44]. Blood samples were collected from healthy volunteers and from individuals with Mediterranean anemia (beta-thalassemia) and stored in sterile containers containing the anticoagulant ethylenediaminetetraacetic acid (EDTA) at a concentration of 1.8 mg/mL of whole blood. The blood was then centrifuged at 2.500 g for 10 min to isolate the erythrocytes, which were subsequently washed three times with phosphate-buffered saline (PBS, pH 7.4).

For the hemolytic evaluation, 1 mL of AgNP0.5, AgNP2.0, at concentrations of 25, 50, 75, and 100 µg/mL were mixed with 1 mL of a 5% erythrocyte suspension in PBS; as negative and positive controls, PBS and 1% sodium dodecyl sulfate (SDS) solution were used in place of the nanoparticle solution, respectively. All the samples were incubated at 37 °C for 2 h and after centrifugated at 2.500 g for 10 min. Hemoglobin release was quantified by

measuring the $A_{540\ nm}$ of the supernatant using the following formula (2).

$$Hemolysis\,(\%) = \left[\frac{A_{AgNPs} - A_0}{A_{SDS} - A_k}\right] \times 100 \quad (2)$$

where $A_{AgNPs\ is}$ the absorbance of samples containing AgNPs, A_0 is the absorbance of the corresponding AgNP concentration in PBS, A_{SDS} is the absorbance of the positive control with SDS, and A_k is the absorbance of the negative control.

Antimicrobial activity assays

Time-kill evaluations

The bactericidal and antibacterial activity of AgNP0.5 and AgNP2.0 was initially evaluated against selected microorganisms: *Staphylococcus aureus* ATCC® 6538, *Pseudomonas aeruginosa* ATCC® 9027, *Salmonella enterica* serovar Typhimurium ATCC® 14028, and *Listeria monocytogenes* ATCC® 19115. The fungicidal and antifungal activity was assessed against *Candida albicans* ATCC® 14053. According to microorganism-specific requirements, single cultures of the five strains were grown under the following conditions: *S. aureus* ATCC® 6538: 24–48 h at 37 °C ; *P. aeruginosa* ATCC® 9027: 24 h at 37 ± 1 °C [45]; *S. enterica* serovar Typhimurium ATCC® 14028: 24 h at 37 ± 1 °C [46]; *L. monocytogenes* ATCC® 19115: 24 h at 37 ± 1 °C [47]; *C. albicans* ATCC® 14053: 48 h at 22 ± 1 °C [48]. Microbial inocula were maintained under constant shaking conditions at 200 rpm in 30 mL tryptic soy broth (TSB, Thermo Fisher Scientific, USA) for bacteria and 30 mL Sabouraud dextrose broth (SAB, Thermo Fisher Scientific, USA) for yeast in sterile tubes with a total volume of 50 mL. To obtain an equal concentration of 10^8 cells/mL of all organisms, the absorbance was measured at 560 nm (bacteria) and 600 nm wavelength (yeast) using a spectrophotometer (Hach Lange DR6000, Hach, USA): an optical density of 1.125 was used as an indicator of 10^9 cells/mL. Inocula were serially diluted to target 10^7 CFU/mL in 10 mL. AgNP0.5 and AgNP2.0 were tested at 100 µg/mL as reported in literature [49]. The experimental protocol was set up according to [50], using the time-kill test [51] to determine the bactericidal or fungicidal effect of the samples to be analysed. The contact time was 3 h (t1) and 20 h (t2). The selected concentrations of the two samples were added to 6-well plates designed to test 0.9% NaCl suspensions of 10 mL of bacteria or yeast, at a microbial load of 10^6 CFU/mL, maintained under constant shaking and at the optimum temperature (37 ± 1 °C for bacteria, 22 ± 1 °C for yeast) for the contact time. Negative controls were prepared using the sole bacterial or yeast inocula without adding AgNPs. Positive controls were prepared by adding $AgNO_3$ at 0.5 mM and 2.0 mM to the bacterial suspension and yeast inoculum. Aliquots were taken shortly after inoculation (t_0) and after the two contact times (t_1 = 3 h, t_2 = 20 h). Antibacterial activity was assessed by determining the number of surviving bacteria in each sample. The residual microbial rate was calculated as CFU/mL measured at two contact times, multiplied by 100, and divided by the microbial concentration (CFU/mL) of the negative control at the corresponding time point. The die-off rate was then determined as follows: 100 - Residual Rate. Microbiological analyses were performed according to ISO guidelines, specific to each microorganism indicated. Selective and specific agar media were used for *S. aureus* (Baird Parker agar base, Thermo Fisher Scientific, USA [52], ; *P. aeruginosa* (*Pseudomonas agar* base, Thermo Fisher Scientific, USA, UNI EN ISO 13720:2010); *S.* Typhimurium (Chromogenic Salmonella agar base, Biolife Italiana, ITALY, ISTISAN 05/27); *L. monocytogenes* (O.A. Listeria agar, Liofilchem, Italy [47]; *C. albicans* (dichloran rose bengal chloramphenicol agar base, Thermo Fisher Scientific, USA [48]. To ensure results reliability, all experiments were performed in independent triplicates. Samples were collected immediately after inoculation (t_0), at 3 h (t_1), and 20 h (t_2) to determine bacteria survival and calculate microbial reduction. Results are reported as mean values ± standard error of the mean (SE) for each nanoparticle tested. ANOVA analysis (GraphPad Prism Software v9, GraphPad Software, La Jolla, CA, USA) was used to determine statistical significance between samples at t_1-t_2 and the negative control at the corresponding time points. p values < 0.05 were considered statistically significant and are indicated in the figures as $^{*}p < 0.05$, $^{**}p < 0.01$, $^{***}p < 0.001$ and $^{****}p < 0.0001$.

MIC determination

MIC of AgNPs was determined using the broth microdilution method, following the guidelines of the Clinical and Laboratory Standards Institute (CLSI) (Zimmer, 2024). The assays were performed in 96-well microplates (Thermo Scientific) with a final volume of 200 µL per well. AgNPs were serially diluted to achieve final concentrations ranging from 100 to 25 µg/mL. Each dilution was mixed with an inoculum containing ~ 2×10^6 CFU/mL of the same target microorganisms used in the time-kill test. As positive and negative controls, $AgNO_3$ and inocula without AgNPs were used. The microplates were incubated for 20 h at 37 °C with continuous shaking (600 rpm). OD measurements were performed using a Thermo Scientific™ Varioskan™ LUX multimode microplate reader. Turbidity readings were taken at 560 nm for bacteria and 590 nm for yeast at t_0 and t_1 = 20 h. All tests were conducted in triplicate. The percentage inhibition of microbial growth was calculated using the following formula:

$$\%\ Growth\ inhibition = 100 \times \left(1 - \frac{A\ 560\ nm\ of\ test\ sample}{A\ 560\ nm\ of\ CTR}\right)$$

An ANOVA analysis was conducted (GraphPad Prism Software version 9 for Windows, GraphPad Software, La Jolla, California, USA, www.graphpad.com) to identify the statistical significance between the sample and Positive Control. P-values < 0.05 were considered statistically significant and are indicated in the graphs as $^{*}p < 0.05$, $^{**}p < 0.01$, $^{***}p < 0.001$, and $^{****}p < 0.0001$.

Catalytic activity of AgNPs

The catalytic activity of synthesized AgNPs was evaluated in the degradation of toxic compounds, including Congo Red (CR) and 4-nitrophenol (4-NP), following the protocols described by Umamaheswari et al. [53] and Desai et al. [54], with minor modifications. For the degradation of CR, the reaction system consisted of 1 mL of AgNP0.5 and AgNP2.0 (at a concentration of 0,05 mg/mL), 1.5 mL of 50 mM $NaBH_4$, and 5 mL of Congo Red (9.4×10^{-5} mM). The progress of the reaction was monitored by measuring changes in the spectra of the reaction mixture over the wavelength range of 600–300 nm at 5-minute intervals, for a total duration of 20 min, in an Agilent Cary UV-Vis spectrophotometer.

For the degradation of 4-NP, 0.5 mL of AgNP0.5 and AgNP2.0 (at a concentration of 0.4 mg/mL) was mixed with 0.5 mL of $NaBH_4$ (1.3 mM) and 5 mL of 4-nitrophenol (7.2×10^{-5} M). Similarly, spectra were recorded in the wavelength range 500–250 nm wavelength at room temperature over 20 min using the same spectrophotometer. Control experiments were conducted in the absence of AgNPs to evaluate the exclusive catalytic effect of $NaBH_4$.

Results and discussion

Factors affecting AgNP formation

Silver nanoparticles (AgNPs) were synthesized using cell-free supernatants of *G. stearothermophilus* GF16, with the secretome acting as a biological matrix to reduce silver ions (Ag^{+}) and determining nanoparticle formation [55]. Several synthesis parameters such as temperature, pH, incubation time, and $AgNO_3$ concentration-were systematically tested to identify the optimal conditions for an efficient AgNP production. As first step, the formation of AgNPs can be verified by observing a color change in the reaction solution, progressing from yellow to increasingly intense brown shades (Fig. 1), which is indicative of nanoparticle formation due to surface plasmon resonance (SPR).

To better investigate the optical properties of the AgNPs, UV-Vis spectra were recorded across the 300–800 nm wavelength range. The spectra revealed SPR peaks with absorption maxima between 410 and 470 nm; SPR peaks located at or below ~430 nm are generally associated with small, spherical silver nanoparticles, whereas peaks above 430 nm suggest the presence of larger particles, anisotropic morphologies, or aggregation phenomena [56]. Peaks extending up to 500 nm further support the formation of irregular or non-spherical nanoparticles. These wavelength shifts are indicative of changes in nanoparticle size, shape, and aggregation state. It is important to note that SPR peak positions are typically referenced for uncoated or stabilized nanoparticles

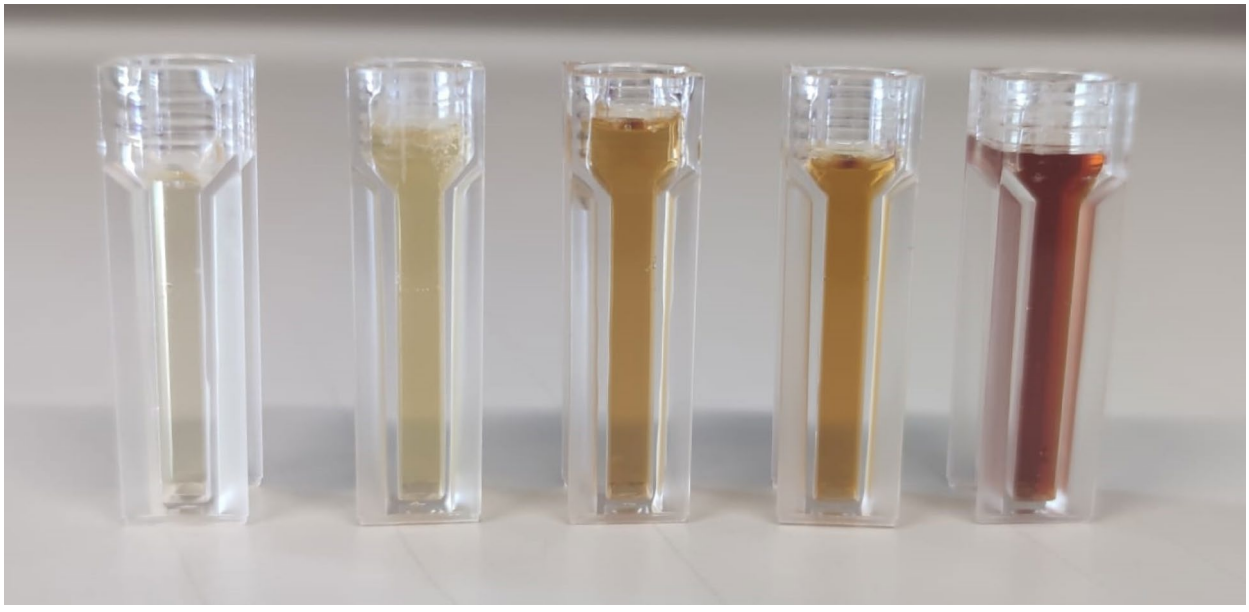

Fig. 1 Colorimetric evidence of AgNP biosynthesis from bacterial secretome. Cuvettes containing the secretome of *G. stearothermophilus* GF16, showing the control (left) and AgNP samples with progressive color changes depending on $AgNO_3$ concentration and incubation time

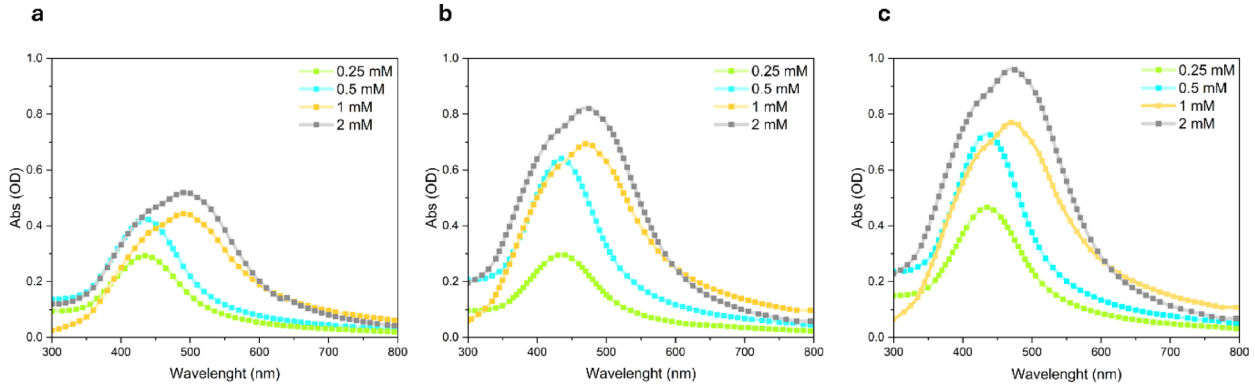

Fig. 2 Effect of temperature on AgNP biosynthesis and plasmonic response. UV–Vis spectra of AgNPs synthesized at 50 °C (a), 60 °C (b), and 80 °C (c) with varying $AgNO_3$ concentrations (0.25–2.0 mM) after 24 h of incubation

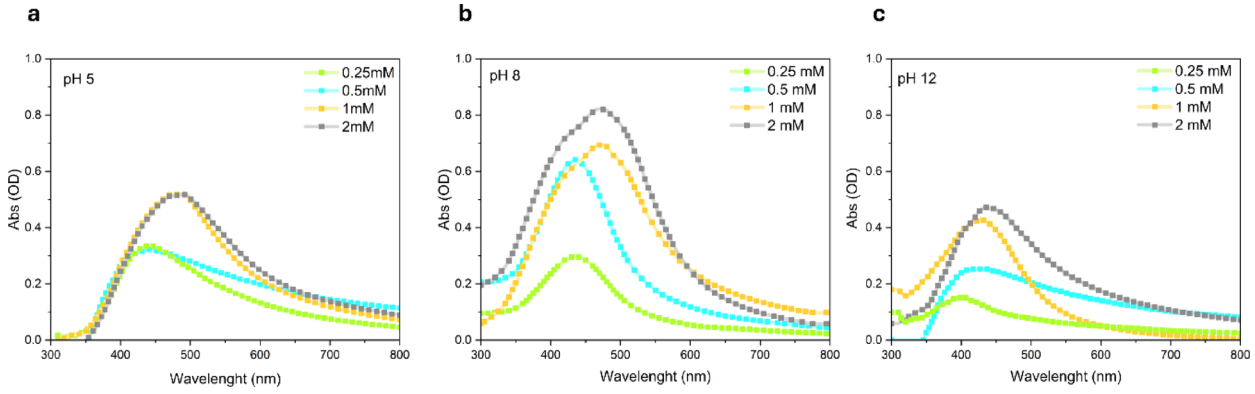

Fig. 3 Effect of pH on AgNP biosynthesis and plasmonic response. UV–Vis absorption spectra of AgNPs synthesized at pH 5 (a), 8 (b), and 12 (c), with $AgNO_3$ concentrations ranging from 0.25 to 2.0 mM after 24 h at 60 °C

[57]. In biologically synthesized AgNPs, however, the organic shell derived from the secretome—composed of proteins, peptides, and other biomolecules—can slightly alter the spectral features by modifying the local refractive index at the nanoparticle surface, leading to minor peak shifts or broadening [58]. Similar SPR profiles have been reported by Al-asbahi et al. [59] who synthesized AgNPs using a mixture of *Lactobacillus sp* and *Bacillus sp*. and observed SPR absorption bands between 410 and 430 nm. Likewise, in another study the production of spherical AgNP mediated by *Bacillus amyloliquefaciens* was confirmed by a peak at 415 nm [60].

To determine the optimal conditions for nanoparticle formation, the effects of various parameters ($AgNO_3$, concentration, T, pH and reaction time) were evaluated. Initially, the secretome was incubated for 24 h with $AgNO_3$ at concentrations of 0.25, 0.5, 1, and 2 mM at temperatures of 25, 37, 50, 60, 70, and 80 °C, and pH 8. After this period, nanoparticle synthesis at 60 °C proved to be the most efficient, as indicated by the higher absorbance between 420 and 470 nm compared to lower temperatures (Fig. 2). At 25 and 37 °C, the synthesis efficiency was lower, as indicated by decreased absorbance values and the nanoparticles formed were smaller, as indicated by a blue-shift in the spectra (Figure S1). At 80 °C nanoparticle synthesis increased (Fig. 2), likely due to the enhanced solubility of $AgNO_3$ and the greater availability of Ag^+ ions in solution; however, the temperature of 60 °C was chosen for subsequent experiments, to reduce energy consumption and improve the sustainability of AgNP synthesis from *G. stearothermophilus* secretomes.

The effect of pH on nanoparticle synthesis was also evaluated. Reactions were conducted for 24 h at pH 5.0 (acidic conditions), 8.0 (the natural pH of the secretome), and 12.0 (basic conditions), at the constant temperature of 60 °C. At each pH level, four $AgNO_3$ concentrations (0.25, 0.5, 1.0 and 2.0) were tested. At pH 5 (Fig. 3), absorption peaks were observed at 435 nm for 0.25 and 0.5 mM $AgNO_3$, and at 490 nm for 1.0 and 2.0 mM $AgNO_3$. At pH 8 (Fig. 3), the observed absorption peaks appeared at 417 nm for lower precursor concentrations (0.25 and 0.5 mM) and around 460 nm for higher concentrations (1.0 and 2.0 mM). At pH 12.0 (Fig. 3), absorption peaks were different for each tested concentration and the absorbance values were always lower than those at pH 8.0, suggesting a less efficient synthesis. We

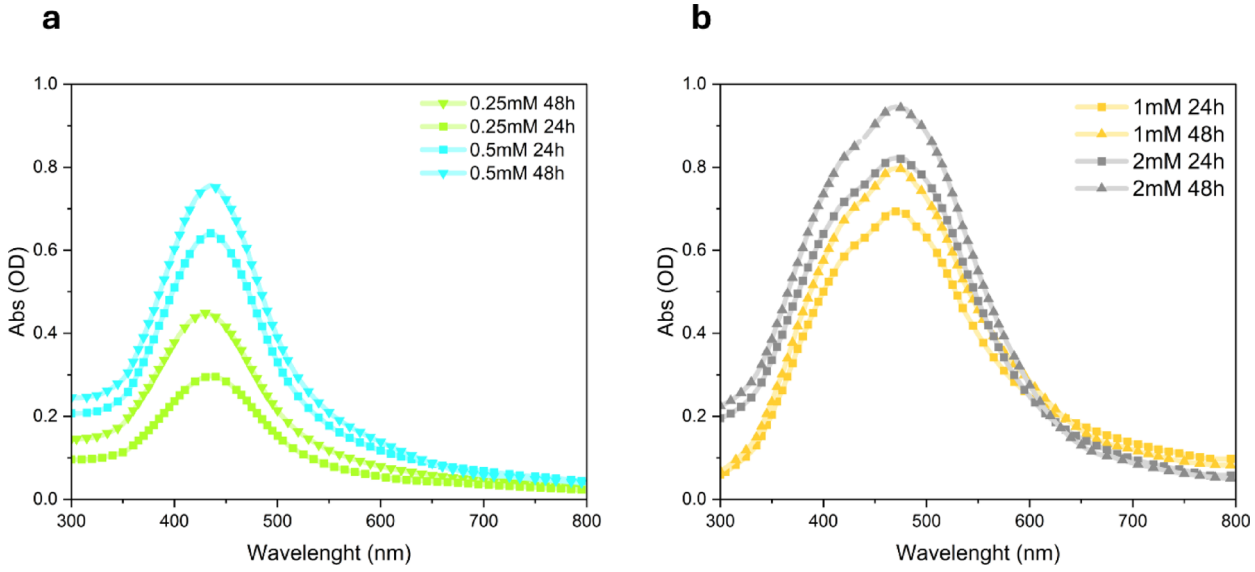

Fig. 4 Effect of reaction time on AgNP biosynthesis. UV–Vis spectra comparing AgNPs synthesized at 60 °C for 24 and 48 h, using $AgNO_3$ at 0.25 and 0.5 mM (a), and 1.0 and 2.0 mM (b)

hypothesized that at this pH value, Ag^+ ions may react with OH^- ions, forming silver hydroxide (AgOH) precipitates, which could subsequently oxidize into silver oxide (Ag_2O), reducing the availability of silver ions for nanoparticle formation. Based on these experiments and considering that lower maximum absorbance values indicate reduced nucleation efficiency, while a redshift in the spectra suggests the formation of larger nanoparticles, pH 8 appeared to offer the most suitable conditions; therefore, it was selected for further characterization.

To investigate the influence of reaction time on nanoparticle formation, similar experiments were conducted using four $AgNO_3$ concentrations (0.25, 0.5, 1.0, and 2.0 mM) at 60 °C, pH 8.0 for 24 and 48 h. As shown in Fig. 4, longer reaction times led to higher absorbance values across all concentrations, indicating an increased nanoparticle yield. Importantly, no significant variations were observed in the absorption maxima, suggesting that the nanoparticle morphology remained unchanged.

Overall, the results demonstrated that, in general, higher temperatures and higher precursor concentrations led to the formation of larger nanoparticles, as evidenced by a redshift in the absorption peak. For example, at 60 °C and pH 8.0 (Fig. 2), higher $AgNO_3$ concentrations (1.0 and 2.0 mM) produced distinct peaks around 470 nm wavelength, indicative of larger nanoparticles, while lower concentrations (0.25 and 0.5 mM) exhibited peaks around 417 nm, corresponding to smaller nanoparticles. Interestingly, at the highest concentrations (1.0–2.0 mM), a distinct shoulder was observed around 417 nm in the UV-Vis spectra, overlapping with the main SPR peak of AgNPs produced at lower concentrations. This suggests the coexistence of two distinct nanoparticle populations with different sizes or morphologies. The broader, redshifted main peak is consistent with partial aggregation or anisotropy. Moreover, biomolecular capping from the secretome may contribute to these spectral features. The presence of a surface coating can modify the local dielectric environment, leading to further SPR broadening or composite peak profiles.

Table 1 Colloidal properties (size and ζ) of synthesized AgNPs

Sample	Size (d. nm)	Đ	ζ (mV)
AgNP0.25	52.2 ± 8.2	0.55 ± 0.03	-10.7 ± 1.3
AgNP0.5	66.0 ± 5.4	0.39 ± 0.05	-18.2 ± 3.1
AgNP2.0	128.4 ± 3.7	0.24 ± 0.05	-24.4 ± 2.1

Characterization by DLS

The colloidal properties of AgNPs synthesized under different conditions were analyzed using DLS, with the results presented in Table 1.

As shown in Table 1, an increase in silver molarity during AgNP synthesis leads to a decrease in zeta potential, resulting in more stable nanoparticles [61]. Regarding the hydrodynamic diameter of the synthesized AgNPs, size distribution decreases as silver molarity increases, as expected by corresponding zeta potential values. Moreover, as silver molarity increased, the particle size also grew, reaching up to 128 nm. It is important to note that the size measured through DLS is generally considered larger than the actual nanoparticle size, as DLS measures the hydrodynamic volume of the particle in solution [62] Representative distribution plots of sample AgNP0.5 and AgNP2.0is reported in Fig. 5.

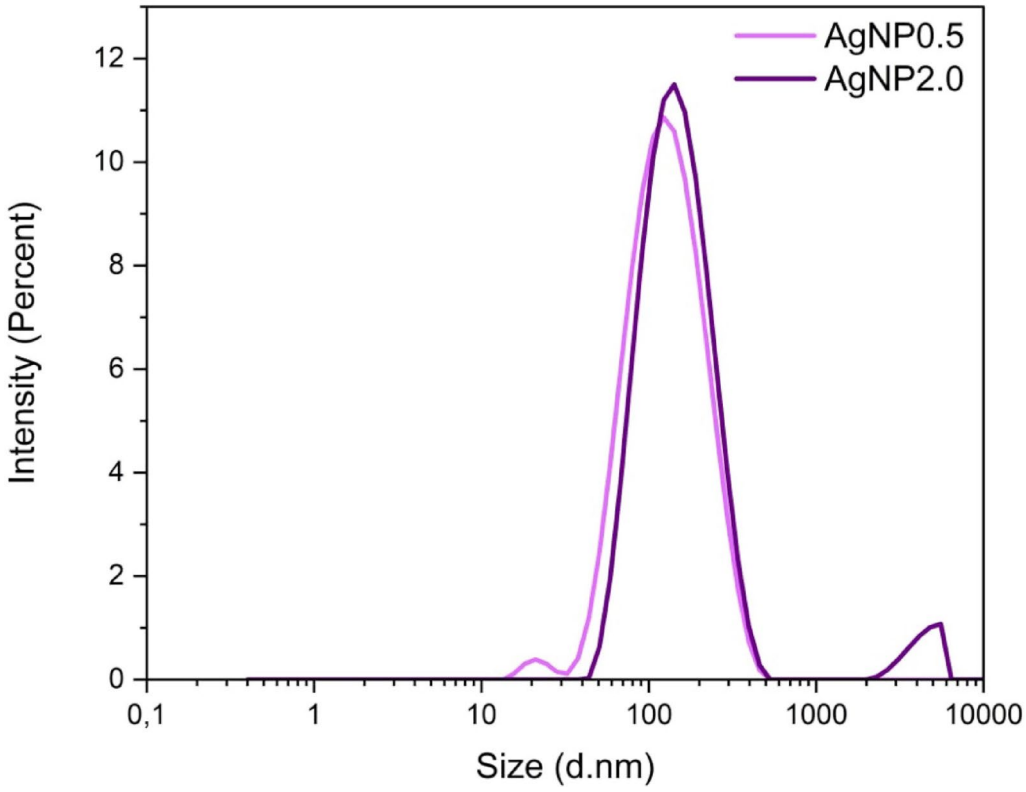

Fig. 5 DLS analysis. Dynamic light scattering (DLS) results showing size distribution by intensity for AgNP0.5 (red) and AgNP2.0 (green)

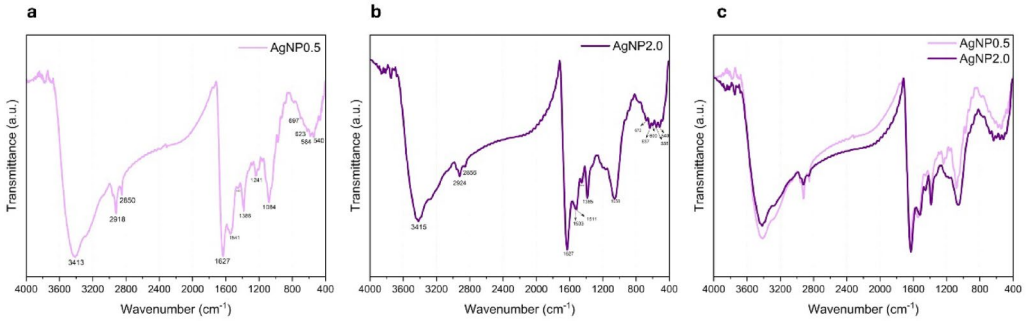

Fig. 6 FTIR analysis. FTIR spectra of AgNP0.5 (a) and AgNP2.0 (b). Panel (c) overlays both spectra to highlight concentration-dependent differences

Characterization of nanoparticle cappings

FTIR analysis was performed to highlight the impact of precursor concentration (0.5 and 2.0 mM $AgNO_3$) on the surface chemistry and interactions in AgNP0.5 and AgNP2. Figure 6 shows differences in the position and intensity of key peaks highlighting that the precursor concentration directly influences the chemical environment and stabilization mechanisms of the nanoparticles [54].

In the aliphatic C-H stretching region, peaks at 2918 and 2850 cm^{-1} (for AgNP0.5) and 2924 and 2856 cm^{-1} (for AgNP2) indicated variations in the organic molecules adsorbed on the nanoparticle surface [63, 64]. The sharper and better-defined peaks of AgNP0.5 suggest a more ordered and structured organic coating, whereas broader and less resolved peaks of AgNP2.0 point to more complex interactions or aggregated molecular layers. Shifts in the fingerprint region, particularly from 1541 to 1533 cm^{-1} and potentially from 1241 to lower wavenumbers, reflect the impact of precursor concentration on the molecular organization at the nanoparticle surface. The band at ~1541 cm^{-1} is attributed to C = C stretching (aromatic rings) and Amide II bending (N–H), while the band at ~1241 cm^{-1} corresponds to C–N stretching from amine or amide groups. These downshifts, moving toward lower frequencies, indicate a reduction in bond vibrational energy, typically resulting from enhanced hydrogen bonding, electrostatic interactions, as well as

denser molecular packing on the nanoparticle surface or coordination with Ag^+ ions [65–67]. At lower precursor concentrations, biomolecules are less densely packed on the nanoparticle surface, allowing functional groups such as C = O, N–H, and C–N to vibrate more freely and maintain higher-energy signals. In contrast, AgNP2.0, show a denser molecular interface promoting hydrogen bonding and stronger interactions with silver ions, restricting bond motion and causing redshifts. Additionally, the emergence of a distinct peak at ~ 1511 cm^{-1}, attributed to N–H bending (Amide II), exclusively in the AgNP2.0 spectrum, supports increased interaction with nitrogen-containing biomolecules [67]. Enhanced intensities of the Amide I band (~ 1627 cm^{-1}, C = O stretching) and C = C aromatic bands (~ 1541 and 1533 cm^{-1}) suggest a greater abundance of proteinaceous or aromatic components adsorbed at higher precursor levels [67, 68]. Finally, low-wavenumber bands at 540 and 584 cm^{-1}, corresponding to Ag–O stretching vibrations, were more pronounced, indicating stronger silver–oxygen interact ions between AgNP2.0 and oxygenated functional groups such as carboxylates or hydroxyls [69]. Altogether, these spectral differences indicate that increasing precursor concentration leads to a more chemically complex and densely coated nanoparticle surface, characterized by stronger molecular binding, lower bond vibrational energies, and enhanced structural stability, features that can be leveraged for improved reactivity and specific surface functionalization [70].

The differences in the FTIR spectra between AgNP0.5 and AgNP2.0 clearly demonstrate the critical role of precursor concentration in determining the surface interactions and chemical environment of AgNPs. At lower precursor concentration, the nanoparticles are characterized by a more defined and ordered organic coating, reflecting simpler surface interactions. This may result in a more predictable and uniform nanoparticle behavior, which therefore might be more suitable for applications requiring precise control of surface properties. In contrast, AgNP2.0 mM exhibits a denser and more complex biomolecular layer, with stronger interactions involving hydroxyl, aromatic, and nitrogenous compounds. This difference either introduces variability in surface properties and could influence colloidal stability and interaction with the surrounding medium; these properties could be advantageous for applications requiring enhanced functionalization or surface activity.

Taken together, the observed variations in surface chemistry suggest that different precursor concentrations can be used to tailor the properties of AgNPs for specific applications. Lower concentrations may be ideal for achieving nanoparticles with well-defined surface interactions, while higher concentrations could be advantageous for generating nanoparticles with enhanced stability and functionalization potential. These findings provide valuable insights into the design and optimization of nanoparticle synthesis protocols for diverse applications, ranging from catalysis to biomedicine.

Table 2 Average size of nanoparticles obtained from different concentrations of $AgNO_3$. The values in the table represent the average size of 100 measured particles, with the standard deviation in parentheses

	SEM	TEM
AgNP0.5	17(± 5)	16(± 5)
AgNP2.0	15(± 5)	16(± 7)

Morphological analysis

The analysis using Electron microscopy, both SEM and TEM, was conducted to examine the morphology of AgNP0.5 and AgNP2.0, and the collected data are in perfect agreement. The analysis confirmed that both samples exhibit a subspherical shape, with slight differences in size (Table 2), while textural differences are clear.

AgNP0.5 exhibits a subspherical shape with an average diameter of 17 nm (Fig. 7A). They are uniformly distributed, and although they form aggregates, they do not overlap. These characteristics could be attributed to a controlled growth process and effective interactions with functional groups on the surface.

AgNP2.0 generally has a subspherical shape too, although in some cases, irregularly shaped particles are observed (Table 2). The irregular morphology is clearly highlighted by the TEM data, which show larger nanoparticle sizes and a higher standard deviation (Table 2). Their average size, 15 nm, is very similar to that of AgNP0.5. However, a significant difference compared to the previous samples lies in their texture: in this case, the nanoparticles are found both isolated, in regular non-overlapping aggregates, and in irregular aggregates. The latter are the most prevalent and show a marked tendency toward particle overlap (Fig. 7B). The greater heterogeneity of this sample, both morphologically and texturally, could be attributed to a less controlled growth process at higher precursor concentration, which may lead to variations in particle shape and distribution. The samples observed under SEM were properly fixed and coated with an Au-Pd alloy, making the resulting images representative not only of the inorganic structures, but also of the organic components potentially present on the particle surfaces. Therefore, the difference between the particle sizes measured by TEM and SEM, which are significantly smaller than those obtained by DLS, is likely due to the sensitivity of the DLS technique to the presence of impurities and aggregates.

Consistent with this interpretation, the SEM and TEM results align with those of FTIR analysis, which suggest

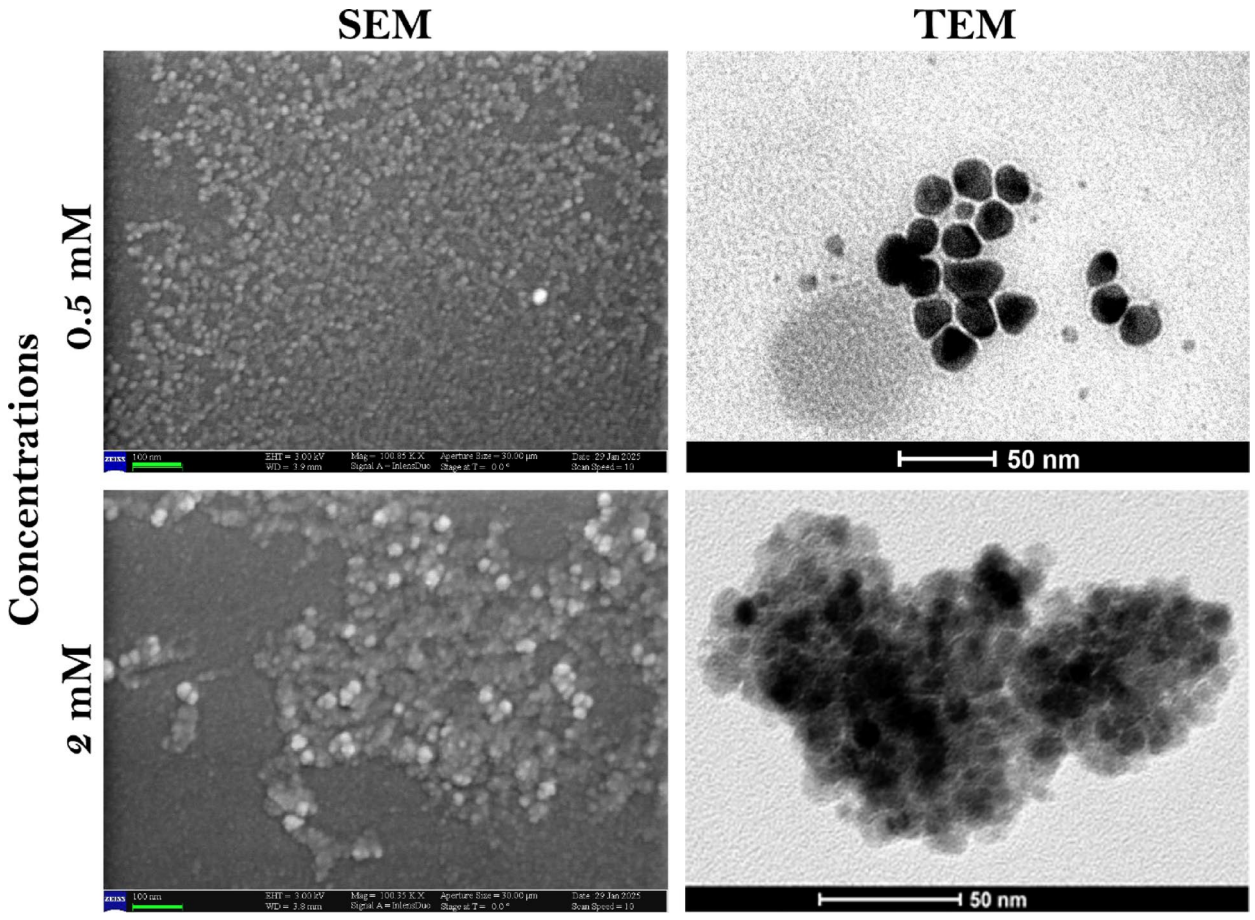

Fig. 7 Morphological characterization via TEM and SEM. Electron micrographs of AgNP0.5 and AgNP2.0, showing changes in aggregation and particle morphology

that AgNP0.5 possess a well-defined organic coating which helps to stabilize and disperse the nanoparticles, thereby reducing aggregation. In contrast, the less structured biomolecular layer, indicated by FTIR for AgNP2.0, could account for the increased aggregation and morphological variability observed.

Thermal stability of biosynthesized AgNPs

The thermal stability of AgNP0.5 and AgNP2.0 was evaluated using isothermal TGA to measure their weight loss profile under autoclave-mimicking conditions, as shown in Fig. 8. The TGA thermograms show that, during the initial heating phase (0–15 min), both samples exhibited a minor weight loss (< 3%), primarily due to the evaporation of residual moisture and weakly bound volatile components [71]. This phenomenon is commonly observed in nanoparticles synthesized in aqueous media, as they tend to retain surface-adsorbed water. Upon reaching the isothermal phase at 120 °C, the weight loss stabilizes, suggesting the absence of further thermal degradation or significant mass loss. These results confirm that both nanoparticle formulations maintain their structural integrity under elevated temperature conditions, demonstrating their thermal stability. A slight variation is observed between the two samples, with AgNP2.0 exhibiting a marginally higher initial weight loss compared to AgNP0.5. This discrepancy may be attributed to the differences already observed in surface chemistry. Moreover, in comparison to other AgNPs derived from plant/mesophilic bacteria, they demonstrated higher thermal stability, possibly due to the presence of heat-resistant biomolecules from *G. stearothermophilus*. These findings highlight the role of biological coating in improving the thermal robustness of AgNPs, which may be advantageous for applications requiring stability at high temperatures. Previous studies have shown that nanoparticles synthesized using plant extracts or mesophilic bacteria often suffer from lower thermal stability due to the degradation of organic molecules involved in their synthesis. Plant-derived nanoparticles, for instance, rely on phytochemicals such as flavonoids, polyphenols, and alkaloids as reducing and stabilizing agents. While these compounds facilitate nanoparticle formation, they may lack the structural resilience required to withstand

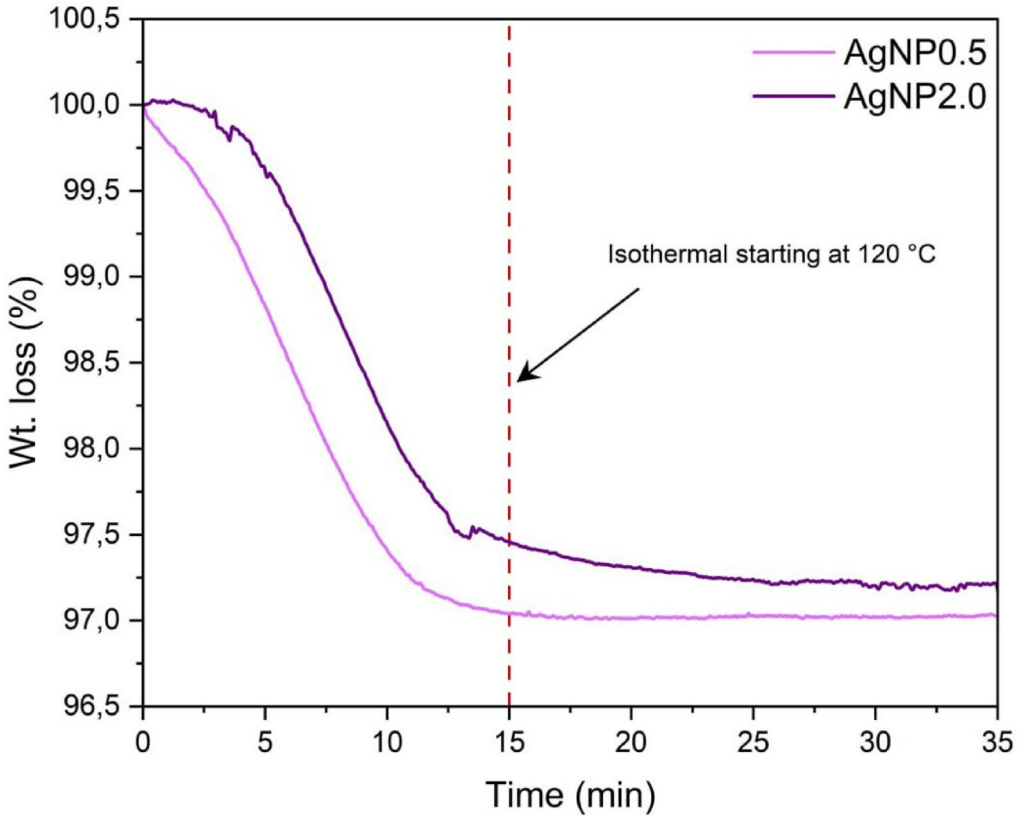

Fig. 8 TGA-based assessment of AgNP thermal stability. Isothermal thermogravimetric analysis showing thermal stability of AgNP0.5 (light pink) and AgNP2.0 (dark purple)

elevated temperatures, leading to nanoparticle aggregation and loss of function over time. Similarly, mesophilic bacteria synthesize AgNPs through enzymatic pathways that involve proteins and extracellular polymeric substances, which may be susceptible to denaturation under high-temperature conditions [72–74]. In contrast, AgNPs synthesized using thermophilic bacteria, such as *G. stearothermophilus*, exhibit superior stability due to the presence of thermostable biomolecules, including heat-resistant proteins and extracellular enzymes that can act as robust capping agents, preventing particle agglomeration and degradation, even under extreme thermal conditions. For example, metallic AgNPs produced using spore extracts from *G. stearothermophilus*, had sizes ranging from 15 to 50 nm and exhibited significant high thermal stability and antimicrobial activity against opportunistic pathogens, indicating their potential application in biomedical and antimicrobial coatings [75].

AgNP antioxidant activity

The antioxidant activity of the cell-free secretome and AgNPs were evaluated assessing their free radical neutralizing capacity in DPPH and ABTS assays. The assays were performed using three different secretome or AgNP concentrations and AgNP0.5 and AgNP2.0 (Fig. 9). As expected, the scavenging activity displayed by the secretome resulted to be concentration dependent with values of 18.0, 8.3, and 3.0% (DPPH) and 18.0, 8.3, and 2.7% (ABTS) at 100, 50, and 25 µg/mL, respectively. The nanoparticles also showed a concentration-dependent scavenging activity, with the highest values observed for AgNP2.0. These reached 79% and 75% scavenging activity in the DPPH and ABTS assays, respectively, in comparison to Trolox, used as the reference antioxidant, which achieved values close to 90% in both assays.

AgNP0.5 exhibited lower antioxidant activity across all tested concentrations, confirming that a higher precursor concentration determines an increased antioxidant capacity. However, when normalized to the silver content, they demonstrated greater efficiency per unit of silver. This means that, although AgNP2.0 show greater absolute antioxidant activity, those produced with 0.5 mM $AgNO_3$ may achieve a comparable effect using a lower precursor concentration. Therefore, in view of large-scale applications the use of lower precursor concentrations not only would reduce material costs but also minimize environmental impact.

These results suggest that bioactive compounds in the secretome, such as polyphenols, along with biomolecules like peptides and proteins may contribute to the

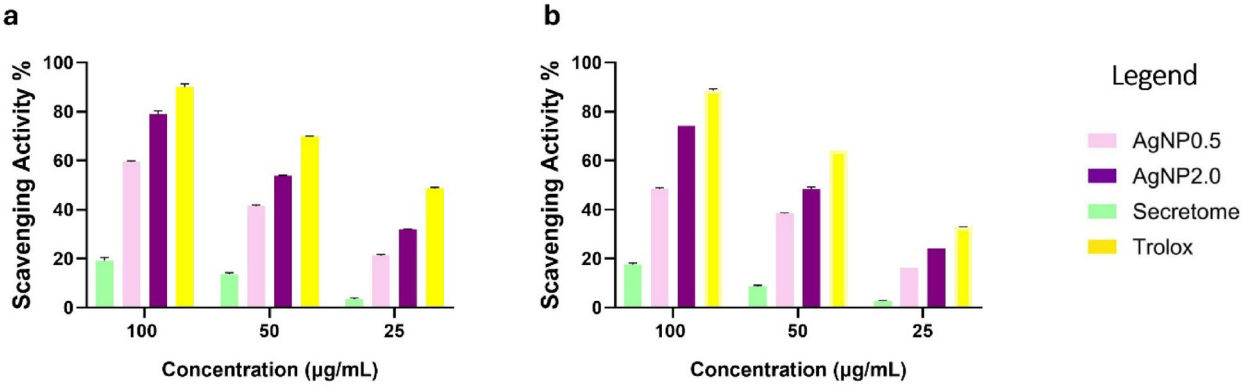

Fig. 9 Antioxidant activity of AgNPs using DPPH and ABTS assays. Antioxidant activity of AgNP0.5 and AgNP2.0 evaluated using (a) DPPH and (b) ABTS assays, compared to secretome and Trolox as reference controls

nanoparticle decoration, enhancing their radical scavenging and metal-chelating properties. Their high surface-to-volume ratio could facilitate interactions with free radicals. Additionally, the biofunctional coating may stabilize reactive intermediates or participate in electron transfer processes, further extending the functionality of the AgNPs [43].

Biosynthesized AgNPs, whether derived from plant extracts [76] or bacterial sources, are increasingly recognized for their significant antioxidant potential [40]. Plant-derived AgNPs, often enriched with polyphenols, have been shown to exhibit superior antioxidant activity compared to their chemically synthesized counterparts [77]. However, bacterial-derived nanoparticles also possess remarkable properties, largely due to their enrichment with other bioactive compounds [78, 79]. In this study, we show for the first time that AgNPs synthesized using *G. stearothermophilus* displayed antioxidant potential comparable to, or even exceeding, that of lactobacillus derived nanoparticles [80]. This is particularly noteworthy, as we also demonstrated that *G. stearothermophilus* nanoparticles possess enhanced thermal stability, attributed to the presence of heat-resistant biomolecules.

These findings underscore the dual advantage of AgNPs synthesized with *G. stearothermophilus*, combining high antioxidant activity with enhanced stability making them a promising alternative to plant- or lactobacilli- derived nanoparticles. Furthermore, AgNP0.5 demonstrated higher efficiency per unit of silver used, highlighting their potential as a more sustainable option for biomedical and environmental applications. Overall, these results emphasize the need to balance antioxidant activity with silver utilization efficiency, paving the way for further studies to optimize synthesis parameters and improve the efficacy of biosynthesized nanoparticles.

Effect of AgNPs on hemolysis rate

To assess the cytotoxicity of the nanoparticles, AgNP0.5 and AgNP2.0, were evaluated in a hemolysis assay performed using both human red blood cells and erythrocytes from individuals with beta-thalassemia. In this assay, erythrocytes were incubated with varying concentrations of nanoparticles (25, 50, 75, and 100 µg/mL) and hemolysis was quantified by measuring the absorbance of hemoglobin at 540 nm after 2 h of incubation at 37 °C. As shown in Fig. 10, the hemolysis increased with nanoparticle concentration but remained below 1% for both cell types; interestingly, these values always remained below the clinical safety threshold of 2% (Table 3), indicating that all the AgNP concentrations tested can be considered safe. However, thalassemic red blood cells showed greater susceptibility to AgNP exposure than healthy cells, likely due to their inherent structural fragility [43, 81].

Overall, the hemolysis data confirms that both AgNP exhibit good hemocompatibility for either healthy or thalassemic cells after 2 h of incubation at 37 °C, highlighting their safety profile. The observed hemolysis rates were lower than those reported for pure metallic nanoparticles [44] which are known to induce cytotoxicity and oxidative stress depending on their size, surface charge, and silver ions release. This improved biocompatibility can be attributed to the natural biomolecular coating of biological AgNPs able to enhance their safety; moreover, this feature makes them a promising candidate for biomedical applications without the need for additional surface interventions. Indeed, a common strategy to improve hemocompatibility and reduce hemolysis involves the functionalization of the nanoparticle surface with organic molecules or polymers, which can also enhance other biological properties, such as the antioxidant potential [82]. Combined with their potential as drug delivery systems, these findings underscore the effectiveness of AgNPs to maintain biological safety even

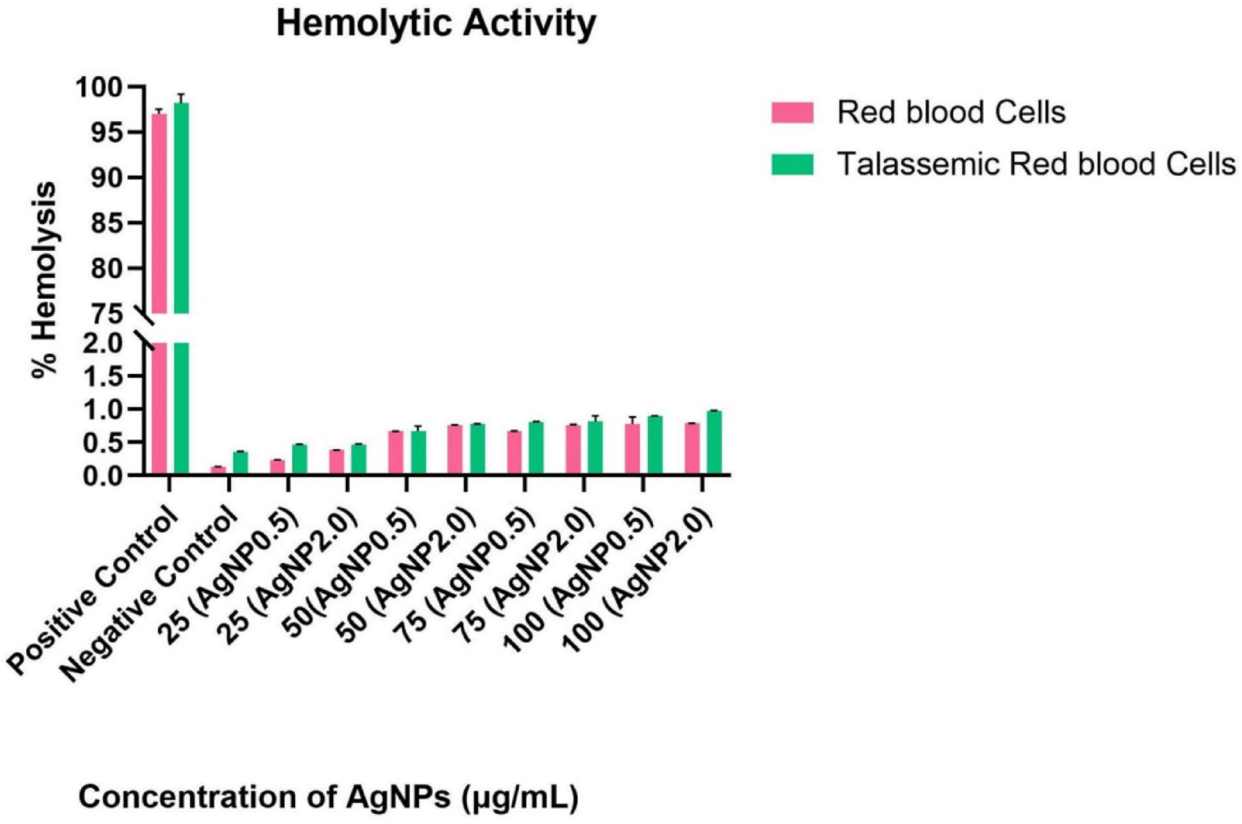

Fig. 10 Hemocompatibility of AgNPs on normal and thalassemic RBCs. Hemolytic activity of AgNP0.5 and AgNP2.0 at concentrations of 25, 50, 75, and 100 µg/mL on normal and β-thalassemic RBCs. Includes positive and negative controls. Mean ± SD from triplicates

Table 3 Hemolytic activity of healthy red blood cells (RBCs) and thalassemic red blood cells exposed to AgNP0.5 and AgNP2.0. Hemolysis percentages were measured at AgNP concentrations of 25, 50, 75, and 100 µg/mL, along with positive and negative controls. Data are presented as mean ± standard deviation, with experiments performed in triplicate. The table highlights the comparative hemolytic responses of healthy and thalassemic RBCs to varying AgNP concentrations

	HEMOLYTIC ACTIVITY	
	Red Blood Cells	**Thalassaemic Red Blood Cells**
Positive control	97.000 ± 0.500	98.2 ± 1.000
Negative control	0.130 ± 0.003	0.36 ± 0.005
25 µg/mL AgNP0.5	0.334 ± 0.005	0.467 ± 0.003
25 µg/mL AgNP2.0	0.381 ± 0.001	0.468 ± 0.010
50 µg/mL AgNP0.5	0.564 ± 0.004	0.672 ± 0.070
50 µg/mL AgNP2.0	0.556 ± 0.005	0.673 ± 0.007
75 µg/mL AgNP0.5	0.669 ± 0.003	0.801 ± 0.010
75 µg/mL AgNP2.0	0.570 ± 0.009	0.811 ± 0.090
100 µg/mL AgNP0.5	0.779 ± 0.100	0.91 ± 0.011
100 µg/mL AgNP2.0	0.782 ± 0.004	0.971 ± 0.007

Table 4 Die-off rate [%] of microorganisms tested at 3 and 20 h with AgNP0.5 and AgNP2.0.5 at 100 ug/ml

Die-off Rate [%]				
Microorganism	**t1 (3 h)**		**t2 (20 h)**	
	AgNP0.5	**AgNP2.0**	**AgNP0.5**	**AgNP2.0**
Staphylococcus aureus ATCC® 6538	34.60	61.48	99.60	100.00
Pseudomonas aeruginosa ATCC® 9027	100.00	96.02	100.00	100.00
Salmonella typhimurium ATCC® 14,028	85.99	26.61	100.00	100.00
Listeria monocytogenes ATCC® 19,115	12.84	2.94	87.19	86.89
Candida albicans ATCC® 14,053	36.78	36.48	85.75	95.58

in diseased red blood cells, confirming their suitability for biomedical applications (Table 3).

Antibacterial efficacy of AgNPs

Bacteria and yeast viability assay

The bacterial viability assay was performed using the bacterial strains of *S. aureus*, *P. aeruginosa*, *S. Typhimurium*, *L. monocytogens* and *C. albicans* after 3- and 20-hours exposure with the AgNP0.5 and AgNP2.0. The bacteria without addition of AgNPs served as the control. Table 4

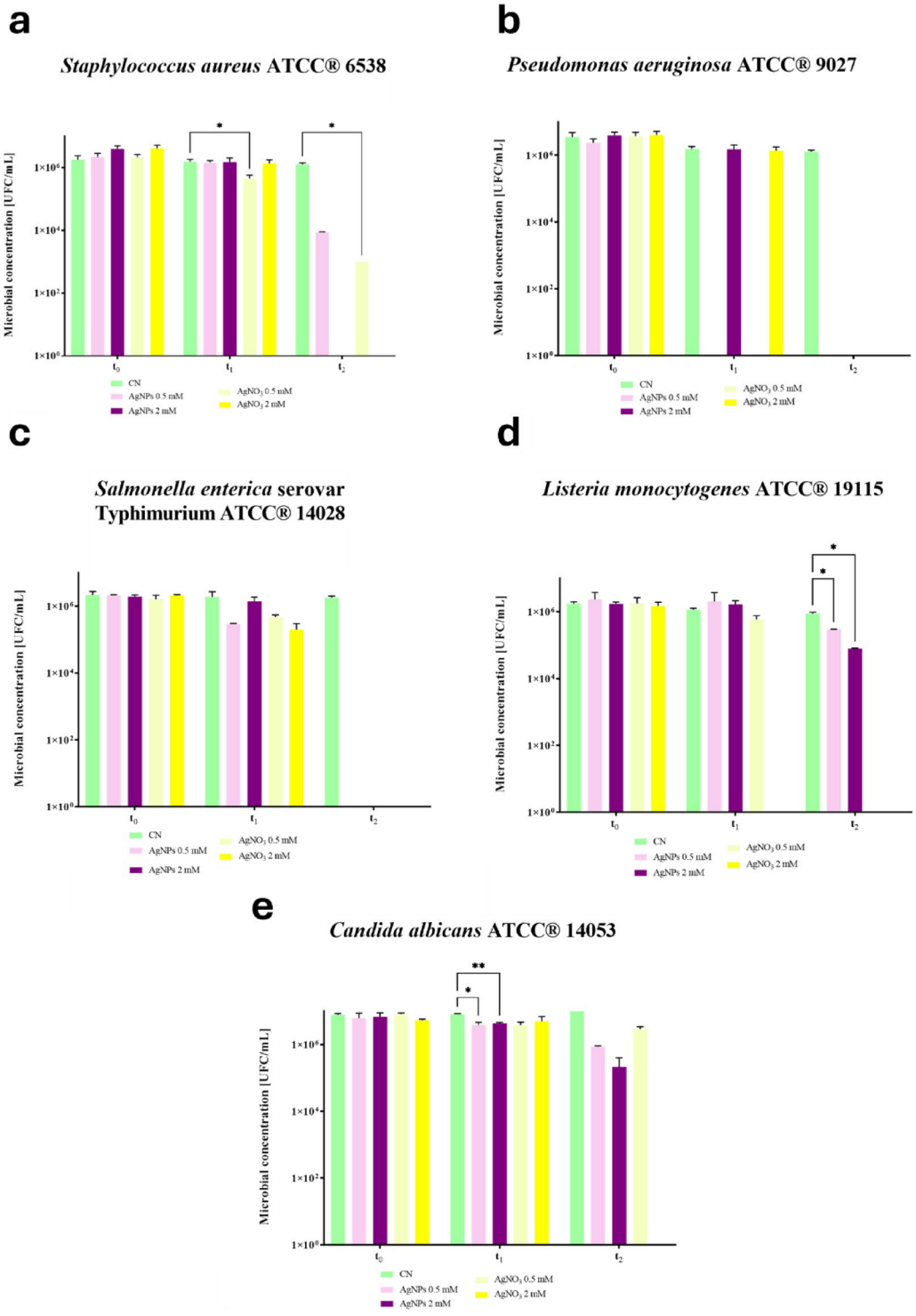

Fig. 11 Antimicrobial activity of AgNPs against bacterial and yeast strains. Effect of AgNP0.5 and AgNP2.0 (100 µg/mL) on pathogens: (a) *S. aureus*, (b) *P. aeruginosa*, (c) S. Typhimurium, (d) *L. monocytogenes*, and (e) *C. albicans*. Data expressed as mean ± SE, with statistical significance

summarizes the data on the die-off rate at 3 and 20 h, while Fig. 11 shows the microbial concentrations at t_1 and t_2 for the different microorganisms tested. The data show that after 3 h of contact, AgNP0.5 and AgNP2.0 (applied at a nanoparticle concentration of 100 µg/ml) do not affect microbial viability, except for *P. aeruginosa*, which shows a 1-log reduction with AgNP2.0 and a complete reduction with AgNP0.5. (Fig. 11 - (b)), and *S. Typhimurium*, which shows a 1-log reduction with AgNP0.5 (Fig. 11 - (c)). After 20 h of contact,

complete elimination of *S. aureus*, *P. aeruginosa* and *S. Typhimurium* is observed, while the microbial load of *L. monocytogenes* and *C. albicans* is reduced by 1 log.

MIC of AgNPs

Based on the promising results obtained in in vitro tests on various microorganisms, the compounds were further analyzed using the MIC test. The MIC test evaluates microbial viability as a function of the optical density detected. In order to determine the lowest concentration at which antimicrobial activity is still present, the compounds were tested at 50 and 25 µg/mL in addition to the 100 µg/mL concentration. Complete (100%) inhibition was confirmed at 100 µg/mL for both AgNP0.5 and AgNP2.0 against *S. aureus* (Fig. 12 - (a)). However, the lower the concentration of AgNP0.5 the weaker the

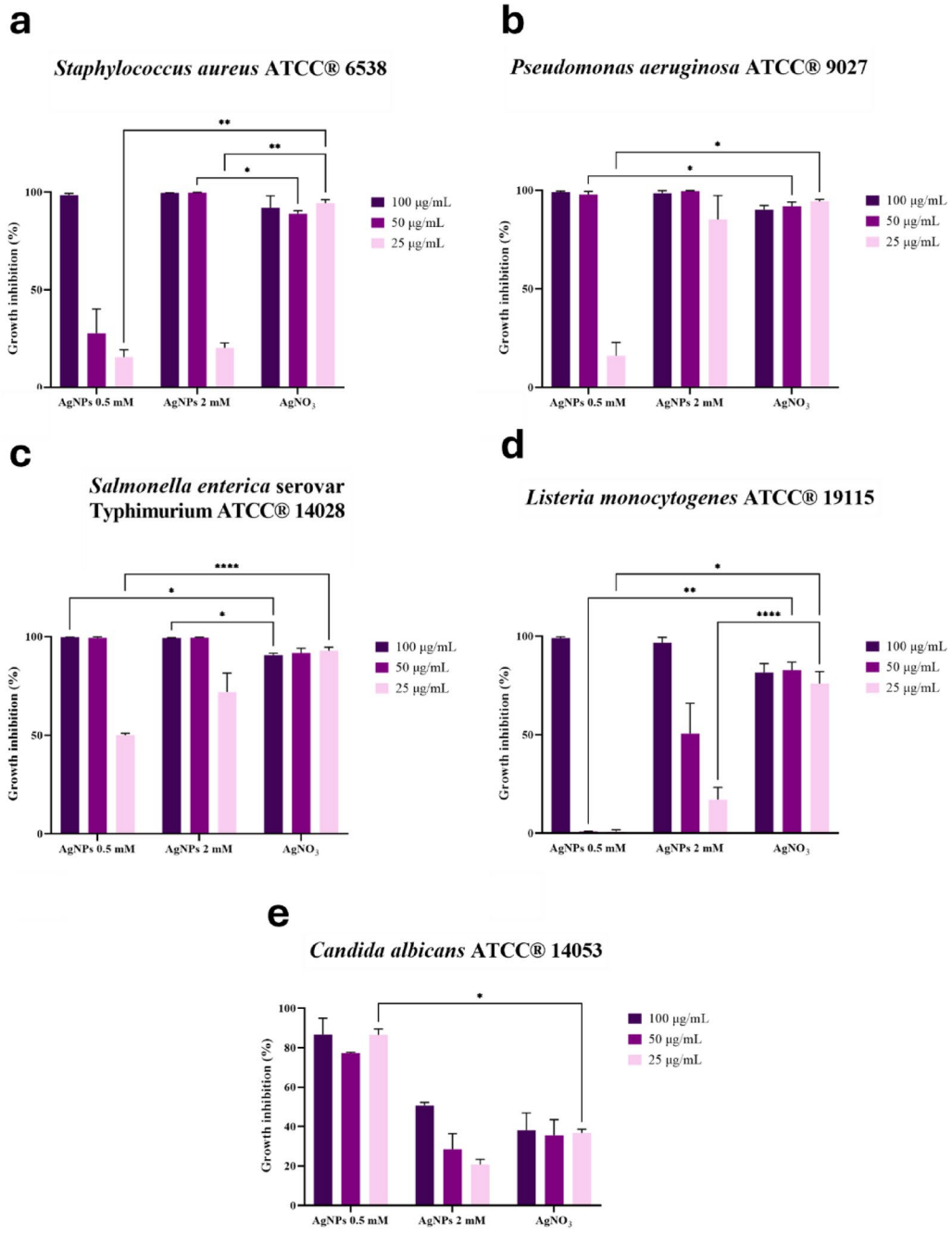

Fig. 12 Dose-dependent antimicrobial activity of AgNPs. Antimicrobial activity of AgNP0.5 and AgNP2.0 (25, 50, and 100 µg/mL) against pathogens: (a) *S. aureus*, (b) *P. aeruginosa*, (c) S. *Typhimurium*, (d) *L. monocytogenes*, and (e) *C. albicans*. Significance levels indicated: *$p < 0.05$, **$p < 0.01$, ***$p < 0.001$, ****$p < 0.0001$

antimicrobial effect. The kill rate is 30% at 50 µg/mL and 15% at 25 µg/mL. Conversely, AgNP2.0 retained high antimicrobial activity at 50 µg/mL, but the mortality rate decreased to 25% at 25 µg/mL. For *P. aeruginosa* (Fig. 12 - (b)), the mortality rate decreased significantly at a concentration of 25 µg/mL, reaching 16% with AgNP0.5 and 85% with AgNP2.0. A similar behaviour was observed for *S. Typhimurium* (Fig. 12 - (c)), where at a concentration of 25 µg/mL the mortality rate was 50% for AgNP0.5 and 71% for AgNP2.0. In the case of *L. monocytogenes* (Fig. 12 - (d)), AgNP0.5 were already ineffective at 50 µg/ml, whereas AgNP2.0 retained an antimicrobial effect with a die-off rate of 50% at 50 µg/ml and 16% at 25 µg/ml. Finally, in the case of *C. albicans* (Fig. 12 - (e)), AgNP0.5 appeared to have a greater effect than AgNP2.0, with a die-off rate of around 80%. This is higher than that observed for the positive control $AgNO_3$, which is around 50%. Overall, the results of the MIC and bacterial viability assays confirmed the strong antimicrobial and antifungal potential of AgNPs across the different microorganisms, highlighting variations in efficacy depending on concentration, exposure time, and microbial species. AgNPs showed the highest activity against *P. aeruginosa*, whereas *L. monocytogenes* was the most resistant. However, even *L. monocytogenes* and *C. albicans*, which displayed higher resilience, showed a significant reduction in microbial load, indicating that AgNPs remain effective against more resistant strains. In general, AgNP2.0 exhibited greater antimicrobial activity compared to those synthesized with 0.5 mM, suggesting a dose-dependent response. The only exception was observed for *C. albicans*, which showed unexpected higher sensitivity to AgNPs synthesized with the lowest precursor concentration. This result suggests that additional factors, such as specific interactions between the nanoparticles and microbial cells, may influence antimicrobial performance. Importantly, when compared with data available in the literature, the AgNPs in this study demonstrate comparable or superior antimicrobial activity. For example, Parvekar et al. [83], reported a MIC value of 625 µg/ml for AgNPs against *Staphylococcus aureus*, whereas in our study, the MIC for this strain was 100 µg/mL. Similar comparisons can be drawn in another study, in which MIC values for spherical AgNPs ranged from 400 to 800 µg/mL for pathogens such as *E. coli* and *S. aureus* [84]. In contrast, in this work AgNPs consistently exhibited lower MIC values against the same strains, confirming their stronger antimicrobial potential. These findings align with the well-documented shape- and size-dependent antimicrobial mechanisms of AgNPs and suggest that the physicochemical properties combined with the biological capping provided by the extremophilic secretome may enhance interactions with microbial cells and promote membrane disruption.

Taken together, these results not only reinforce the broad-spectrum antimicrobial efficacy of silver nanoparticles, but also highlight their potential applications in clinical, pharmaceutical, and environmental fields. Further studies are necessary to enhance their selectivity and optimize treatment parameters, to ultimately support the development of targeted AgNP-based antimicrobial formulations.

Catalytic efficiency of AgNPs

Nanoparticle technology has emerged as a promising pre-treatment approach for wastewater treatment, facilitating the degradation of organic contaminants and improving their biodegradability for further downstream processing. Among the various nanocatalysts explored, biogenic nanoparticles synthesized using bacteria have demonstrated significant potential in environmental remediation. To address this issue, the catalytic efficiency of AgNPs was evaluated in the degradation of toxic compounds, specifically Congo Red (CR) and 4-nitrophenol (4-NP) and the results are shown in Fig. 13. Without the addition of AgNPs, the degradation of both compounds in the presence of the reducing agent $NaBH_4$ was extremely slow (Fig. 13a, d). This indicates that $NaBH_4$ alone is not sufficient to drive the reduction reaction efficiently. Conversely, the addition of synthesized AgNP0.5 and AgNP2.0 significantly accelerated the degradation of both CR and 4-NP, as evidenced by the rapid decline in the absorbance of their characteristic UV-Vis peaks (Fig. 13b-c, and 13e-f) confirming their high catalytic activity.

In particular, the CR solution exhibited a strong initial absorbance between 400 and 500 nm, corresponding to the characteristic π-π transitions of the azo (-N = N-) bonds. Upon the addition of AgNPs, the reduction reaction was markedly accelerated, leading to a gradual disappearance of the absorbance peak and a visible color change from red to colorless within 20 min. This transformation is attributed to the electron transfer from the borohydride ion (BH_4^-), dissociated from $NaBH_4$, to the azo group of CR, a process facilitated by AgNPs acting as electron mediators.

Similarly, in the case of 4-NP, a strong absorbance peak at ~400 nm, characteristic of the nitro group (-NO_2), progressively decreased over time in the presence of AgNPs indicating the reduction of 4-NP to 4-aminophenol (4-AP), whose absorption shifts towards lower wavelengths (~300 nm).

A study reported that copper oxide nanoparticles derived from *Escherichia* sp. were effective in treating textile wastewater, achieving 97.07% degradation of CR within 5 h under direct sunlight exposure [85]. In contrast, this study demonstrates that AgNPs catalyze the almost complete degradation of CR in much less time

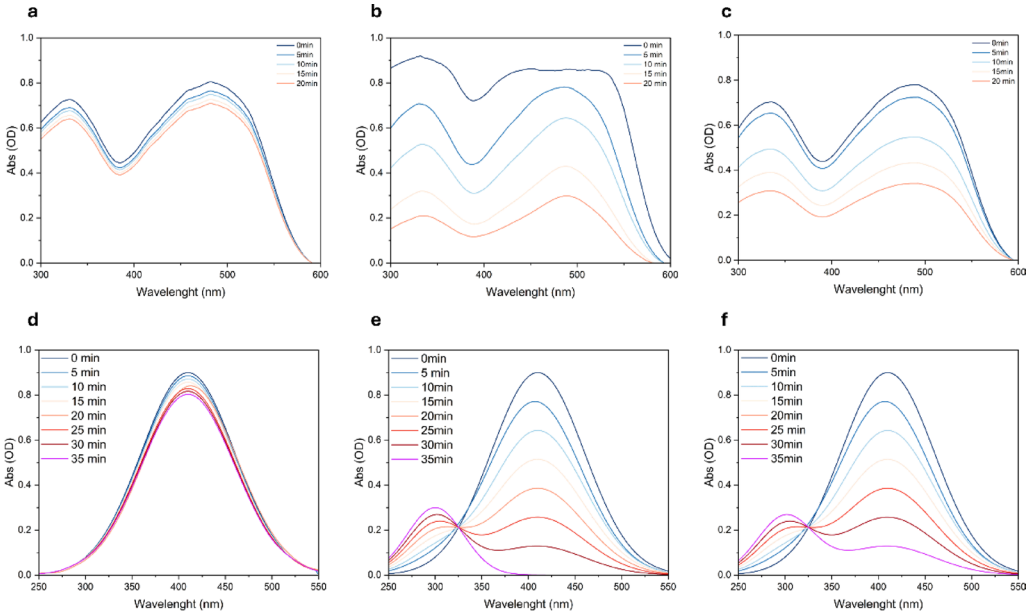

Fig. 13 Catalytic degradation of CR and 4-NP by AgNPs. UV–Vis spectra showing CR (a, b, c) or 4-NP (d, e, f) degradation in presence of $NaBH_4$: (a, d) control, (b, e) AgNP0.5 AgNP2.0, (c, f) AgNP2.0. CR degradation was monitored over 20 min, while 4-NP degradation was monitored over 35 min

i.e. within 20 min, showing their higher catalytic activity. The rapid electron transfer from $NaBH_4$ to the azo (-N = N-) bonds of CR, facilitated by AgNPs, led to an accelerated reduction reaction, making them a highly effective alternative for more rapid wastewater treatment. Gold nanoparticles (AuNPs) derived from *Pseudomonas lipolytica* have also been investigated for their role in the decolorization of CR through an electron transfer mechanism mediated by $NaBH_4$. These studies indicated that AuNPs exhibited high catalytic efficiency for CR degradation compared to AgNPs, likely due to their superior electron transfer properties and surface stability [86]. However, our findings revealed that AgNPs successfully catalyzed the rapid reduction of CR within 20 min, demonstrating comparable catalytic properties at a significantly lower cost. Several other nanocatalysts have been also investigated for 4-NP reduction, including AuNPs and palladium nanoparticles. AuNPs have been widely studied for their stability and efficiency in mediating electron transfer during 4-NP reduction. Also in this case, the high cost of gold limits its practical application [87].

To better understand the degradation mechanism, the reaction kinetics for CR and 4-NP were analyzed as a function of time, maintaining a constant temperature of 25 °C and using $NaBH_4$ in excess to prevent it from being the limiting factor. The role of AgNPs is important in facilitating the transfer of electrons from BH_4^- to the substrates promoting their reduction. Experimental data were fitted to three kinetic models: zero-, first-, and second-order. The analysis and the derived correlation coefficient (R^2, Table S2) revealed that in both cases, the pseudo-zero-order model best describes the mechanism and rate of catalytic degradation and is consistent with previous studies on the use of metal nanoparticles in the degradation of synthetic dyes. The results obtained underscore the tremendous potential of AgNP0.5 and AgNP2.0 in treating toxic compounds resistant to biodegradation. Their ability to accelerate reduction reactions and transform hazardous molecules into less harmful products represents a significant step forward in the development of sustainable nanocatalysts.

Conclusions

This study presents the first complete physicochemical characterization of AgNPs biosynthesized using the cell-free secretome of *G. stearothermophilus* GF16, a thermophilic and cadmium-resistant bacterium isolated from a hydrothermal volcanic area. By optimizing key synthesis parameters such as silver nitrate concentration, temperature, pH, and reaction time we demonstrated that *G. stearothermophilus* GF16 acts as a dynamic, flexible and efficient microbial chassis for the green production of AgNPs with controlled size, morphology, and surface properties.

A key strength of this system lies in its cost-effectiveness and simplicity: nanoparticles were synthesized using only a basic, non-specialized growth medium, without the need for expensive inducers, complex additives, or nitrate supplementation. The secretome alone was sufficient to drive reduction and stabilization, making the process highly sustainable and reproducible.

The resulting AgNPs exhibited an exceptional combination of functional properties: up to 79% DPPH and 75%

ABTS scavenging activity, thermal stability up to 120 °C, and broad-spectrum antimicrobial efficacy, including complete inhibition of *Staphylococcus aureus*, *Pseudomonas aeruginosa*, and *Salmonella Typhimurium* at 100 µg/mL. In addition, catalytic degradation of Congo Red and 4-nitrophenol was achieved within 20 and 35 min, respectively. Notably, the AgNPs also demonstrated excellent hemocompatibility, with hemolysis rates below 1%, even in β-thalassemic erythrocytes.

Altogether, our results confirm the scientific novelty and applied potential of using thermophilic secretomes as dual reducing and capping agents in nanomaterial synthesis. *G. stearothermophilus* GF16 emerges as a robust, flexible, and eco-sustainable nanofactory, capable of producing multifunctional AgNPs with superior antioxidant, antimicrobial, and catalytic performance compared to literature benchmarks. This platform paves the way for scalable applications in precision nanomedicine, green catalysis, and antimicrobial technologies, while contributing to sustainable and low-impact innovation in nanobiotechnology. Future work will focus on cytotoxicity evaluations in human cell lines to further establish the biocompatibility of these nanoparticles and support their advancement toward clinical and biomedical applications.

Abbreviations

4-AP	4-aminophenol
4-NP	4-nitrophenol
ABTS	2,2′-azino-bis(3-ethylbenzothiazoline-6-sulfonic acid)
ANOVA	Analysis of Variance
AgNPs	Silver Nanoparticles
CFU/mL	Colony Forming Units per milliliter
CR	Congo Red
DLS	Dynamic Light Scattering
DPPH	2,2-diphenyl-1-picrylhydrazyl
EDS	Energy Dispersive X-ray Spectroscopy
FTIR	Fourier-Transform Infrared Spectroscopy
GF16	Geobacillus stearothermophilus GF16
ISO	International Organization for Standardization
LB	Lysogeny Broth
MIC	Minimum Inhibitory Concentration
OD	Optical Density
PBS	Phosphate-Buffered Saline
SD	Standard Deviation
SDGs	Sustainable Development Goals
SDS	Sodium Dodecyl Sulfate
SEM / FeSEM	Scanning Electron Microscopy / Field Emission SEM
SPR	Surface Plasmon Resonance
TEM	Transmission Electron Microscopy
TGA	Thermogravimetric Analysis
UV-Vis	Ultraviolet–Visible Spectroscopy

Supplementary Information

The online version contains supplementary material available at https://doi.org/10.1186/s12934-025-02815-9.

Supplementary Material 1.

Supplementary Material 2.

Acknowledgements

We gratefully acknowledge Dr Sergio Sorbo and Dr Antonella Giarra for assisting in the preparation of samples for electron microscopy and image acquisition.

Author contributions

P.C., M.G., D.L: conceptualization; V.S.: conceptualization and data curation; F.C.: conceptualization, data curation and validation; M.R.: data curation and validation; M.S.: methodology and data curation; G.D.P.: conceptualization, methodology, data curation and validation; G.F.: writing – original draft, supervision, funding acquisition, data curation, methodology and validation; A.D.F.: writing – original draft, methodology, data curation, conceptualization. All authors reviewed the manuscript.

Funding

This work was partially funded by Ministero dell'Università e della Ricerca, PRIN 2022 AGRI-FOOD CHIP Agri-food CHains Integration Project. CUP: E53C24003120006.

Data availability

The data used to support the findings of this study are available within the paper. The genomic sequence of G. stearothermophilus GF16 is available on NCBI database with accession number: NZ_RCTI01000001. Raw data files are also available on request from the corresponding author upon reasonable request.

Declarations

Consent for publication

Not applicable.

Competing interests

The authors declare no competing interests.

Author details

[1]Department of Biology, University of Naples Federico II, Naples, Italy
[2]Institute of Polymers, Composites and Biomaterials, National Research Council, Pozzuoli, Italy
[3]Institute of Crystallography, Department of Chemical Sciences and Materials Technology, National Research Council, Rome, Italy
[4]Department of Earth Sciences, Environment and Resources, University of Naples Federico II, Naples, Italy

Received: 27 May 2025 / Accepted: 2 August 2025
Published online: 19 August 2025

References

1. Guilger-Casagrande M, Germano-Costa T, Bilesky-José N, Pasquoto-Stigliani T, Carvalho L, Fraceto LF, et al. Influence of the capping of biogenic silver nanoparticles on their toxicity and mechanism of action towards sclerotinia sclerotiorum. J Nanobiotechnol 24 Febbraio. 2021;19(1):53.
2. Pasquoto-Stigliani T, Guilger-Casagrande M, Campos EVR, Germano-Costa T, Bilesky-José N, Migliorini BB, et al. Titanium biogenic nanoparticles to help the growth of trichoderma Harzianum to be used in biological control. J Nanobiotechnol 25 Maggio. 2023;21(1):166.
3. Nyandoro VO, Masioge HK, Malago ZL. Biogenic synthesis of metal nanoparticles: promoting green nanotechnology and sustainable development goals. Clean Techn Environ Policy. 2024. https://doi.org/10.1007/s10098-024-02966-0. https://link.springer.com/. Accessed 12 Nov 2024.
4. Di Fraia S, Di Meglio A, Massarotti N, Vanoli L, Bentivoglio R, Volpecina V. Energy recovery and waste valorization in a frozen food processing facility: a case study from lazio, Italy. Energy Effi Marzo. 2024;17(3):13.
5. Puri A, Mohite P, Maitra S, Subramaniyan V, Kumarasamy V, Uti DE, et al. From nature to nanotechnology: the interplay of traditional medicine, green chemistry, and biogenic metallic phytonanoparticles in modern healthcare innovation and sustainability. Biomed Pharmacotherapy Gennaio. 2024;170:116083.
6. Griffo R, Di Natale F, Minale M, Sirignano M, Parisi A, Carotenuto C. Analysis of carbon nanoparticle coatings via wettability. Nanomaterials 1 Febbraio. 2024;14(3):301.

7. Siddiqi KS, Husen A, Rao RAK. A review on biosynthesis of silver nanoparticles and their biocidal properties. J Nanobiotechnol Dicembre. 2018;16(1):14.
8. Piluk T (Dorothy), Faccio G, Letsiou S, Liang R, Freire-Gormaly M, editors. A critical review investigating the use of nanoparticles in cosmetic skin products. Environ Sci: Nano. 2024;11(9):3674–92.
9. Okaiyeto K, Gigliobianco MR, Di Martino P. Biogenic zinc oxide nanoparticles as a promising antibacterial agent: synthesis and characterization. IJMS. 2024;25(17):9500.
10. Vijayaram S, Razafindralambo H, Sun YZ, Vasantharaj S, Ghafarifarsani H, Hoseinifar SH, et al. Applications of green synthesized metal Nanoparticles — a review. Biol Trace Elem Res Gennaio. 2024;202(1):360–86.
11. Durán N, Silveira CP, Durán M, Martinez DST. Silver nanoparticle protein Corona and toxicity: a mini-review. J Nanobiotechnol Dicembre. 2015;13(1):55.
12. EL-Zawawy NA, Abou-Zeid AM, Beltagy DM, Hantera NH, Nouh HS. Mycosynthesis of silver nanoparticles from endophytic Aspergillus flavipes AUMC 15772: ovat-statistical optimization, characterization and biological activities. Microb Cell Fact 6 Novembre. 2023;22(1):228.
13. El.Fadly EB, Salah AS, Abdella B, Al Ali A, AlShmrany H, ElBaz AM, et al. Mapping a sustainable approach: biosynthesis of lactobacilli-silver nanocomposites using whey-based medium for antimicrobial and bioactivity applications. Microb Cell Fact 6 Luglio. 2024;23(1):195.
14. Kajani AA, Bordbar AK, Zarkesh Esfahani SH, Razmjou A. Gold nanoparticles as potent anticancer agent: green synthesis, characterization, and in vitro study. RSC Adv. 2016;6(68):63973–83.
15. Dang KPT, Nguyen TTG, Cao TD, Le VD, Dang CH, Duy NPH, et al. Biogenic fabrication of a gold nanoparticle sensor for detection of Fe^{3+} ions using a smartphone and machine learning. RSC Adv. 2024;14(29):20466–78.
16. Burketová L, Martinec J, Siegel J, Macůrková A, Maryška L, Valentová O. Noble metal nanoparticles in agriculture: impacts on plants, associated microorganisms, and biotechnological practices. Biotechnol Adv Settembre. 2022;58:107929.
17. Jeyaraj M, Gurunathan S, Qasim M, Kang MH, Kim JH. A comprehensive review on the synthesis, characterization, and biomedical application of platinum nanoparticles. Nanomaterials 2 Dicembre. 2019;9(12):1719.
18. Wang YL, Lee YH, Chou CL, Chang YS, Liu WC, Chiu HW. Oxidative stress and potential effects of metal nanoparticles: A review of biocompatibility and toxicity concerns. Environ Pollution Aprile. 2024;346:123617.
19. Pomerantseva E, Bonaccorso F, Feng X, Cui Y, Gogotsi Y. Energy storage: the future enabled by nanomaterials. Sci 22 Novembre. 2019;366(6468):eaan8285.
20. Vodyanoy V. The role of endogenous metal nanoparticles in biological systems. Biomolecules 23 Ottobre. 2021;11(11):1574.
21. Darwesh OM, Marzoog A, Matter IA, Okla MK, El-Tayeb MA, Aufy M, et al. Natural dyes developed by microbial-nanosilver to produce antimicrobial and anticancer textiles. Microb Cell Fact 2 Luglio. 2024;23(1):189.
22. Kalakonda P, Thodeti M, Ganneboina C, Ankathi K, Kathri S, Begari K et al. Eco-friendly fabrication of silver nanoparticles for sustainable water purification and antibacterial synergy. Plasmonics. 2024. https://doi.org/10.1007/s11468-024-02251-2. https://link.springer.com/. Accessed 12 Nov 2024.
23. Tan P, Li H, Wang J, Gopinath SCB. Silver nanoparticle in biosensor and bioimaging: clinical perspectives. Biotechnology and applied biochemistry. 2020;11:bab.2045.
24. Jangid H, Singh S, Kashyap P, Singh A, Kumar G. Advancing biomedical applications: an in-depth analysis of silver nanoparticles in antimicrobial, anticancer, and wound healing roles. Front Pharmacol 8 Agosto. 2024;15:1438227.
25. Biswas K, Ahamed Z, Dutta T, Mallick B, Khuda-Bukhsh AR, Biswas JK, et al. Green synthesis of silver nanoparticles from waste leaves of tea (Camellia sinensis) and their catalytic potential for degradation of Azo dyes. J Mol Struct Dicembre. 2024;1318:139448.
26. Baraketi S, Khwaldia K. Nanoparticles from agri-food by-products: green technology synthesis and application in food packaging. Curr Opin Green Sustainable Chem Ottobre. 2024;49:100953.
27. Ratan ZA, Haidere MF, Nurunnabi Md S, SMd, Ahammad AJS, Shim YY, et al. Green chemistry synthesis of silver nanoparticles and their potential anticancer effects. Cancers 1 Aprile. 2020;12(4):855.
28. Perumalsamy H, Balusamy SR, Sukweenadhi J, Nag S, MubarakAli D, El-Agamy Farh M, et al. A comprehensive review on Moringa Oleifera nanoparticles: importance of polyphenols in nanoparticle synthesis, nanoparticle efficacy and their applications. J Nanobiotechnol 19 Febbraio. 2024;22(1):71.
29. Laib I, Ali BD, Alsalme A, Croun D, Bechelany M, Barhoum A. Therapeutic potential of silver nanoparticles from Helianthemum lippii extract for mitigating cadmium-induced hepatotoxicity: liver function parameters, oxidative stress, and histopathology in Wistar rats. Front Bioeng Biotechnol 27 Giugno. 2024;12:1400542.
30. Srisrimal DA, Mohandoss DKD, Srisrimal A, Darshakumar RD, Prabhu S, Tamarakar S, et al. Silver nanoparticles: evaluation of in vivo toxicity in rats. BioNanoSci Marzo. 2023;13(1):176–85.
31. Goel M, Sharma A, Sharma B. Recent advances in biogenic silver nanoparticles for their biomedical applications. Sustainable Chem 3 Marzo. 2023;4(1):61–94.
32. Jadoun S, Chauhan NPS, Zarrintaj P, Barani M, Varma RS, Chinnam S, et al. Synthesis of nanoparticles using microorganisms and their applications: a review. Environ Chem Lett Ottobre. 2022;20(5):3153–97.
33. Beeler E, Singh OV. Extremophiles as sources of inorganic bio-nanoparticles. World J Microbiol Biotechnol. 2016;32(9). http://link.springer.com/https://doi.org/10.1007/s11274-016-2111-7. Accessed 14 July 2025.
34. Aulitto M, Gallo G, Puopolo R, Mormone A, Limauro D, Contursi P et al. Genomic insight of Alicyclobacillus Mali FL18 isolated from an Arsenic-Rich hot spring. Front Microbiol. 2021. https://doi.org/10.3389/fmicb.2021.639697/full. https://www.frontiersin.org/articles/. Accessed 14 July 2025.
35. Antonucci I, Gallo G, Limauro D, Contursi P, Ribeiro AL, Blesa A et al. An ArsR/SmtB family member regulates arsenic resistance genes unusually arranged in *Thermus thermophilus* HB27. Microbial Biotechnol. 2017;10(6):1690–701.
36. Mohammed Fayaz A, Girilal M, Rahman M, Venkatesan R, Kalaichelvan PT. Biosynthesis of silver and gold nanoparticles using thermophilic bacterium Geobacillus stearothermophilus. Process Biochem Ottobre. 2011;46(10):1958–62.
37. Puopolo R, Gallo G, Mormone A, Limauro D, Contursi P, Piochi M et al. Identification of a new heavy-metal-resistant strain of *Geobacillus stearothermophilus* isolated from a hydrothermally active volcanic area in Southern Italy. IJERPH. 2020;17(8):2678.
38. Carbonaro M, Aulitto M, Mazurkewich S, Fraia AD, Contursi P, Limauro D, et al. Genomic mining of Geobacillus stearothermophilus GF16 for xylose production from hemicellulose-rich biomasses using secreted enzymes. New Biotechnol Settembre. 2024;82:14–24.
39. Gallo G, Zannini D, Immirzi B, De Bruno A, Fiorentino G, Dal Poggetto G. Host–guest complexes HP-β-CD/citrus antioxidants: exploratory evaluations of enhanced properties in biodegradable film packaging. Antioxidants. 2023;12(3):763.
40. Bedlovičová Z, Strapáč I, Baláž M, Salayová A. A brief overview on antioxidant activity determination of silver nanoparticles. Molecules 13 Luglio. 2020;25(14):3191.
41. Chu SC, Chen C. Effects of origins and fermentation time on the antioxidant activities of Kombucha. Food Chem Gennaio. 2006;98(3):502–7.
42. Xiao F, Xu T, Lu B. Guidelines for antioxidant assays for food components.
43. Srećković NZ, Nedić ZP, Monti DM, D'Elia L, Dimitrijević SB, Mihailović NR, et al. Biosynthesis of silver nanoparticles using salvia pratensis L. Aerial part and root extracts: bioactivity, biocompatibility, and catalytic potential. Molecules 1 Febbraio. 2023;28(3):1387.
44. Yedgar S, Barshtein G, Gural A. Hemolytic Activity of Nanoparticles as a Marker of Their Hemocompatibility. Micromachines. 2022;13(12):2091.
45. ISO. ISO 13720:2010. https://www.iso.org/standard/45099.html. Accessed 10 Mar 2025.
46. ISO. ISO 6579-1:2017. https://www.iso.org/standard/56712.html. Accessed 10 Mar 2025.
47. ISO. ISO 11290-1:2017. https://www.iso.org/standard/60313.html. Accessed 10 Mar 2025.
48. ISO. ISO 21527-1:2008. https://www.iso.org/standard/38275.html. Accessed 10 Mar 2025.
49. Mythili R, Selvankumar T, Srinivasan P, Sengottaiyan A, Sabastinraj J, Ameen F, et al. Biogenic synthesis, characterization and antibacterial activity of gold nanoparticles synthesised from vegetable waste. J Mol Liquids Luglio. 2018;262:318–21.
50. Standards E. European Standards | BSI Standards | International Standards. https://www.en-standard.eu/. Accessed 10 Mar 2025.
51. Alrashidi A, Jafar M, Higgins N, Mulligan C, Varricchio C, Moseley R et al. A time-kill assay study on the synergistic bactericidal activity of pomegranate rind extract and Zn (II) against methicillin-resistant *Staphylococcus aureus* (MRSA), *Staphylococcus epidermidis*, *Escherichia coli*, and *Pseudomonas aeruginosa*. Biomolecules. 2021;11(12):1889.
52. ISO. ISO 6888-1:2021. https://www.iso.org/standard/76672.html. Accessed 7 Mar 2025.
53. Umamaheswari C, Lakshmanan A, Nagarajan NS. Green synthesis, characterization and catalytic degradation studies of gold nanoparticles against congo

red and Methyl orange. J Photochem Photobiology B: Biology Gennaio. 2018;178:33–9.
54. Desai MP, Patil RV, Pawar KD. Green biogenic approach to optimized biosynthesis of noble metal nanoparticles with potential catalytic, antioxidant and antihaemolytic activities. Process Biochem Novembre. 2020;98:172–82.
55. Lavecchia R, García-Martínez JB, Contreras-Ropero JE, Barajas-Solano AF, Zuorro A. Antibacterial and photocatalytic applications of silver nanoparticles synthesized from *Lacticaseibacillus rhamnosus*. IJMS. 2024;25(21):11809.
56. Paramelle D, Sadovoy A, Gorelik S, Free P, Hobley J, Fernig DG. A rapid method to estimate the concentration of citrate capped silver nanoparticles from UV-visible light spectra. Analyst 1 Luglio. 2014;139(19):4855.
57. Solís-Sandí I, Cordero-Fuentes S, Pereira-Reyes R, Vega-Baudrit JR, Batista-Menezes D. Montes de Oca-Vásquez G. Optimization of the biosynthesis of silver nanoparticles using bacterial extracts and their antimicrobial potential. Biotechnol Rep Dicembre. 2023;40:e00816.
58. Kim DH, Park JC, Jeon GE, Kim CS, Seo JH. Effect of the size and shape of silver nanoparticles on bacterial growth and metabolism by monitoring optical density and fluorescence intensity. Biotechnol Bioproc E Aprile. 2017;22(2):210–7.
59. Al-asbahi MGSS, Al-Ofiry BA, Saad FAA, Alnehia A, Al-Gunaid MQA. Silver nanoparticles biosynthesis using mixture of Lactobacillus sp. and Bacillus sp. growth and their antibacterial activity. Sci Rep 3 Maggio. 2024;14(1):10224.
60. Eid AM, Hassan SED, Hamza MF, Selim S, Almuhayawi MS, Alruhaili MH, et al. Photocatalytic, antimicrobial, and cytotoxic efficacy of biogenic silver nanoparticles fabricated by Bacillus amyloliquefaciens. Catalysts 30 Giugno. 2024;14(7):419.
61. Chouhan S, Guleria S. Green synthesis of AgNPs using cannabis sativa leaf extract: characterization, antibacterial, anti-yeast and α-amylase inhibitory activity. Mater Sci Energy Technol. 2020;3:536–44.
62. Gurunathan S. Biologically synthesized silver nanoparticles enhances antibiotic activity against Gram-negative bacteria. J Industrial Eng Chem Settembre. 2015;29:217–26.
63. Viola V, Allah P, Perumal P, Catauro M. Alkali activation of Metakaolin and wollastonite: reducing sodium hydroxide use and enhancing gel formation through carbonation. Mater 8 Ottobre. 2024;17(19):4910.
64. Hussein FA, Hussien NN, Jabir MS, Ghotekar S, Swelum AA. Biogenic synthesized silver nanoparticles for control of multidrug resistant bacteria, and Inhibition of NLRP3 inflammasome activation: In-vitro- and in-vivo study. Inorg Chem Commun Gennaio. 2025;171:113567.
65. Das R, Kumar P, Singh AK, Agrawal S, Albukhaty S, Bhattacharya I et al. Green synthesis of silver nanoparticles using *Trema Orientalis* (L.) extract and evaluation of their antibacterial activity. Green Chem Lett Rev. 2025;18(1):2444679.
66. Catauro M, Viola V, D'Amore A. Mosses on geopolymers: preliminary durability study and chemical characterization of metakaolin-based geopolymers filled with wood ash. Polymers. 2023;15(7):1639.
67. Shandiz SAS, Hashemi A, Rezaei N, Haghani B, Baghbani-Arani F. Cytotoxic activity of silver nanoparticles prepared by eco-friendly synthesis using lythrum salicaria extract on breast cancer cells. Mol Biol Rep Dicembre. 2025;52(1):18.
68. Petrelli V, Dell'Anna MM, Mastrorilli P, Viola V, Catauro M, D'Angelo A. Synthesis by Sol–Gel route of Organic–Inorganic hybrid material: chemical characterization and in vitro release study. Appl Sci 20 Luglio. 2023;13(14):8410.
69. Viola V, D'Angelo A, Vertuccio L, Catauro M. Metakaolin-based geopolymers filled with industrial wastes: improvement of physicochemical properties through sustainable waste recycling. Polymers. 2024;16(15):2118.
70. Wan Mat Khalir WKA, Shameli K, Jazayeri SD, Othman NA, Che Jusoh NW, Hassan NM. Biosynthesized silver nanoparticles by aqueous stem extract of Entada spiralis and screening of their biomedical activity. Front Chem 19 Agosto. 2020;8:620.
71. Viola V, Catauro M, D'Amore A, Perumal P. Assessing the carbonation potential of wood ash for CO2 sequestration. Low-carbon Mater Green Constr. 2024;2(1):12.
72. Fayaz AM, Balaji K, Girilal M, Yadav R, Kalaichelvan PT, Venketesan R. Biogenic synthesis of silver nanoparticles and their synergistic effect with antibiotics: a study against gram-positive and gram-negative bacteria. Nanomedicine: Nanatechnol Biology Med Febbraio. 2010;6(1):103–9.
73. Iravani S. Bacteria in nanoparticle synthesis: current status and future prospects. Int Sch Res Notices 29 Ottobre. 2014;2014:1–18.
74. Tiquia-Arashiro S, Rodrigues D. Thermophiles and psychrophiles in nanotechnology. In: Extremophiles: applications in nanotechnology. Cham: Springer International Publishing; 2016. pp. 89–127. http://link.springer.com/https://doi.org/10.1007/978-3-319-45215-9_3. Accessed 6 Mar 2025.
75. Yazdian-Robati R, Hedayati N, Ramezani M, Abnous K, Taghdisi SM. Colorimetric gold nanoparticles-based aptasensors. Nanomed J. 2018;5(1). https://doi.org/10.22038/nmj.2018.05.001
76. Nirmala C, Sridevi M. Characterization, antimicrobial and antioxidant evaluation of biofabricated silver nanoparticles from endophytic Pantoea anthophila. J Inorg Organomet Polym Settembre. 2021;31(9):3711–25.
77. Reddy NJ, Nagoor Vali D, Rani M, Rani SS. Evaluation of antioxidant, antibacterial and cytotoxic effects of green synthesized silver nanoparticles by Piper longum fruit. Mater Sci Engineering: C Gennaio. 2014;34:115–22.
78. Riaz Rajoka MS, Mehwish HM, Zhang H, Ashraf M, Fang H, Zeng X, et al. Antibacterial and antioxidant activity of exopolysaccharide mediated silver nanoparticle synthesized by Lactobacillus brevis isolated from Chinese Koumiss. Colloids Surf B: Biointerfaces Febbraio. 2020;186:110734.
79. Abishad P, Vergis J, Unni V, Ram VP, Niveditha P, Yasur J, et al. Green synthesized silver nanoparticles using Lactobacillus acidophilus as an antioxidant, antimicrobial, and antibiofilm agent against Multi-drug resistant enteroaggregative Escherichia coli. Probiotics Antimicro Prot Ottobre. 2022;14(5):904–14.
80. Zeinivand M, Aghaei SS, Zargar M, Ghasemzadeh MA. Exopolysaccharide-mediated silver nanoparticles synthesized from Lactobacillus paracasei with antimicrobial, antibiofilm and antioxidant activities. Arch Microbiol Maggio. 2023;205(5):210.
81. Nai A, Cordero-Sanchez C, Tanzi E, Pagani A, Silvestri L, Di Modica SM. Cellular and animal models for the investigation of β-thalassemia. Blood Cells Molecules Dis Gennaio. 2024;104:102761.
82. Bharti S, Mukherji S, Mukherji S. Enhanced antibacterial activity of decahedral silver nanoparticles. J Nanopart Res Febbraio. 2021;23(2):36.
83. Parvekar P, Palaskar J, Metgud S, Maria R, Dutta S. The minimum inhibitory concentration (MIC) and minimum bactericidal concentration (MBC) of silver nanoparticles against *Staphylococcus aureus*. Biomaterial Investigations Dentistry 1 Gennaio. 2020;7(1):105–9.
84. Jp Y. S K. Characterization and antibacterial activity of synthesized silver and iron nanoparticles using Aloe Vera. J Nanomed Nanotechnol. 2016;7(3). https://www.omicsonline.org/open-access/characterization-and-antibacterial-activity-of-synthesized-silver-and-ironnanoparticles-using-aloe-vera-2157-7439-1000384.php?aid=75302. Accessed 28 Mar 2025.
85. Noman M, Shahid M, Ahmed T, Niazi MBK, Hussain S, Song F, et al. Use of biogenic copper nanoparticles synthesized from a native Escherichia sp. as photocatalysts for Azo dye degradation and treatment of textile effluents. Environ Pollution Febbraio. 2020;257:113514.
86. Kulkarni R, Harip S, Kumar AR, Deobagkar D, Zinjarde S. Peptide stabilized gold and silver nanoparticles derived from the Mangrove isolate pseudoalteromonas lipolytica mediate dye decolorization. Colloids Surf A: Physicochemical Eng Aspects Ottobre. 2018;555:180–90.
87. Zhu N, Cao Y, Shi C, Wu P, Ma H. Biorecovery of gold as nanoparticles and its catalytic activities for p-nitrophenol degradation. Environ Sci Pollut Res Aprile. 2016;23(8):7627–38.

Publisher's Note